



International Agreement Report

Verification of RELAP5/MOD 3 With Theoretical and Numerical Stability Results on Single-Phase, Natural Circulation in a Simple Loop

Prepared by
J. C. Ferreri, ARN
W. Ambrosini, USP

Autoridad Regulatoria Nuclear
Av. del Libertador 8250
1429 Buenos, Aires, Argentina

Universita degli Studi di Pisa, Facolta di Ingegneria
Dipartimento di Costruzioni Meccaniche e Nucleari
Via Diotalvi 2, 56126 Pisa, Italy

Office of Nuclear Regulatory Research
U.S. Nuclear Regulatory Commission
Washington, DC 20555-0001

February 1999

Prepared as part of
The Agreement on Research Participation and Technical Exchange
under the International Code Application and Maintenance Program (CAMP)

Published by
U.S. Nuclear Regulatory Commission

AVAILABILITY NOTICE

Availability of Reference Materials Cited in NRC Publications

NRC publications in the NUREG series, NRC regulations, and *Title 10, Energy, of the Code of Federal Regulations*, may be purchased from one of the following sources:

1. The Superintendent of Documents
U.S. Government Printing Office
P.O. Box 37082
Washington, DC 20402-9328
<http://www.access.gpo.gov/su_docs>
202-512-1800
2. The National Technical Information Service
Springfield, VA 22161-0002
<<http://www.ntis.gov/ordernow>>
703-487-4650

The NUREG series comprises (1) technical and administrative reports, including those prepared for international agreements, (2) brochures, (3) proceedings of conferences and workshops, (4) adjudications and other issuances of the Commission and Atomic Safety and Licensing Boards, and (5) books.

A single copy of each NRC draft report is available free, to the extent of supply, upon written request as follows:

Address: Office of the Chief Information Officer
Reproduction and Distribution
Services Section
U.S. Nuclear Regulatory Commission
Washington, DC 20555-0001
E-mail: <GRW1@NRC.GOV>
Facsimile: 301-415-2289

A portion of NRC regulatory and technical information is available at NRC's World Wide Web site:

<<http://www.nrc.gov>>

All NRC documents released to the public are available for inspection or copying for a fee, in paper, microfiche, or, in some cases, diskette, from the Public Document Room (PDR):

NRC Public Document Room
2121 L Street, N.W., Lower Level
Washington, DC 20555-0001
<<http://www.nrc.gov/NRC/PDR/pdr1.htm>>
1-800-397-4209 or locally 202-634-3273

Microfiche of most NRC documents made publicly available since January 1981 may be found in the Local Public Document Rooms (LPDRs) located in the vicinity of nuclear power plants. The locations of the LPDRs may be obtained from the PDR (see previous paragraph) or through:

<<http://www.nrc.gov/NRC/NUREGS/SR1350/V9/lpdr/html>>

Publicly released documents include, to name a few, NUREG-series reports; *Federal Register* notices; applicant, licensee, and vendor documents and correspondence; NRC correspondence and internal memoranda; bulletins and information notices; inspection and investigation reports; licensee event reports; and Commission papers and their attachments.

Documents available from public and special technical libraries include all open literature items, such as books, journal articles, and transactions, *Federal Register* notices, Federal and State legislation, and congressional reports. Such documents as theses, dissertations, foreign reports and translations, and non-NRC conference proceedings may be purchased from their sponsoring organization.

Copies of industry codes and standards used in a substantive manner in the NRC regulatory process are maintained at the NRC Library, Two White Flint North, 11545 Rockville Pike, Rockville, MD 20852-2738. These standards are available in the library for reference use by the public. Codes and standards are usually copyrighted and may be purchased from the originating organization or, if they are American National Standards, from—

American National Standards Institute
11 West 42nd Street
New York, NY 10036-8002
<<http://www.ansi.org>>
212-642-4900

DISCLAIMER

This report was prepared under an international cooperative agreement for the exchange of technical information. Neither the United States Government nor any agency thereof, nor any of their employees, makes any warranty, expressed or implied, or assumes any legal liability or responsibility for any third

party's use, or the results of such use, of any information, apparatus, product, or process disclosed in this report, or represents that its use by such third party would not infringe privately owned rights.

NUREG/IA-0151



International Agreement Report

Verification of RELAP5/MOD 3 With Theoretical and Numerical Stability Results on Single-Phase, Natural Circulation in a Simple Loop

Prepared by
J. C. Ferreri, ARN
W. Ambrosini, USP

Autoridad Regulatoria Nuclear
Av. del Libertador 8250
1429 Buenos, Aires, Argentina

Universita degli Studi di Pisa, Facolta di Ingegneria
Dipartimento di Costruzioni Meccaniche e Nucleari
Via Diotisalvi 2, 56126 Pisa, Italy

Office of Nuclear Regulatory Research
U.S. Nuclear Regulatory Commission
Washington, DC 20555-0001

February 1999

Prepared as part of
The Agreement on Research Participation and Technical Exchange
under the International Code Application and Maintenance Program (CAMP)

Published by
U.S. Nuclear Regulatory Commission

**VERIFICATION OF RELAP5/MOD3
WITH THEORETICAL AND NUMERICAL STABILITY RESULTS
on single-phase, natural circulation in a simple loop**

ABSTRACT

The theoretical results given by Pierre Welander [1] are used to test the capability of the RELAP5 series of codes to predict instabilities in single-phase flow. These results are related to the natural circulation in a loop formed by two parallel adiabatic tubes with a point heat sink at the top and a point heat source at the bottom. A stability curve may be defined for laminar flow and was extended to consider turbulent flow. By a suitable selection of the ratio of the total buoyancy force in the loop to the friction resistance, the flow may show instabilities. The solution was useful to test two basic numerical properties of the RELAP5 code, namely: a) convergence to steady state flow-rate using a "lumped parameter" approximation to both the heat source and sink and, b) the effect of nodalization to numerically damp the instabilities. It was shown that, using a single volume to lump the heat source and sink, it was not possible to reach convergence to steady state flow rate when the heated (cooled) length was diminished and the heat transfer coefficient increased to keep constant the total heat transferred to (and removed from) the fluid. An algebraic justification of these results is presented, showing that it is a limitation inherent to the numerical scheme adopted. Concerning the effect of nodalization on the damping of instabilities, it was shown that a "reasonably fine" discretization led, as expected, to the damping of the solution. However, the search for convergence of numerical and theoretical results was successful, showing the expected nearly chaotic behavior. This search led to very refined nodalizations. The results obtained have also been verified by the use of simple, ad hoc codes. A procedure to assess the effects of nodalizations on the prediction of instabilities threshold is outlined in this report. It is based on the experience gained with the aforementioned simpler codes.

CONTENTS

Abstract	iii
Contents	v
List of Tables	vii
List of Figures	vii
Executive Summary	xi
Acknowledgments	xiii
Nomenclature	xv
I. Introduction	1
II. Theoretical Analysis	2
III. Numerical Results	6
IV. Conclusions	14
References	15
APPENDIX A	26
Internal Memorandum on "Limitations of the Use of Heat Exchanger Approximation for a Point Heat Source"	
APPENDIX B	38
Theoretical Stability Analysis for Turbulent Natural Circulation in a Simple Loop	
APPENDIX C	43
-Results From the Application of RELAP5/MOD3.x Code Plots of Selected Results	
-List of Cases Considered and Their Nodalizations	
APPENDIX D	64
Input Deck for Welander's Problem	

LIST OF TABLES

Table 1 Specification of a Test Problem

LIST OF FIGURES

- Figure C.1a** TEST #1 Base Case using **RELAP5/MOD3.0**
Mass Flow Rates in Legs and TDV junction, 10 nodes per leg,
(Length of Components = 1m, Heated Length = 1m,
Initial Mass Flow Rate=0.1Kg/s)
- Figure C.1b** TEST #1 Base Case
Fluid Temperatures at Source, Ascending Leg Cell 5,
Sink and Descending Leg Cell 5, conditions as in Figure C.1a.
- Figure C.2a** TEST #2 Sensitivity of results to heated length using **RELAP5/MOD3.0**
Mass Flow Rates in Legs and TDV junction, 10 nodes per leg,
(Length of Components = 1m, Heated Length = 0.5m,
Initial Mass Flow Rate=0.1Kg/s)
- Figure C.2b** TEST #2 Sensitivity of results to heated length
Fluid Temperatures at Source, Ascending Leg Cell 5,
Sink and Descending Leg Cell 5, conditions as in Figure C.2a.
- Figure C.3a** TEST #3 Sensitivity of results to heated length using **RELAP5/MOD3.0**
Mass Flow Rates in Legs and TDV junction, 10 nodes per leg,
(Length of Components = 1m, Heated Length = 0.1m,
Initial Mass Flow Rate=0.1Kg/s)
- Figure C.3b** TEST #3 Sensitivity of results to heated length
Fluid Temperatures at Source, Ascending Leg Cell 5,
Sink and Descending Leg Cell 5, conditions as in Figure C.3a.
- Figure C.4a** TEST #4 Sensitivity of results to node number using **RELAP5/MOD3.0**
Mass Flow Rates in Legs and TDV junction, 25 nodes per leg,
(Length of Components = 0.4m, Heated Length = 0.1m,
Initial Mass Flow Rate=0.1Kg/s)
- Figure C.4b** TEST #4 Sensitivity of results to node number
Fluid Temperatures at Source, Ascending Leg Cell 5,
Sink and Descending Leg Cell 5, conditions as in Figure C.4a.
- Figure C.5a** TEST #5 Sensitivity of results to node number using **RELAP5/MOD3.0**
Mass Flow Rates in Legs and TDV junction, 50 nodes per leg,
(Length of Components = 0.2m, Heated Length = 0.1m,
Initial Mass Flow Rate=0.1Kg/s)
- Figure C.5b** TEST #5 Sensitivity of results to node number

Fluid Temperatures at Source, Ascending Leg Cell 5,
Sink and Descending Leg Cell 5, conditions as in Figure C.5a.

- Figure C.6a** TEST #6 The recovery of unstable behavior using **RELAP5/MOD3.0**
Mass Flow Rates in Legs and TDV junction, 90 nodes per leg,
(Length of Components = 0.11m, Heated Length = 0.1m,
Initial Mass Flow Rate = 0.1Kg/s)
- Figure C.6b** TEST #6 The recovery of unstable behavior
Fluid Temperatures at Source, Ascending Leg Cell 5,
Sink and Descending Leg Cell 5, conditions as in Figure C.6a.
- Figure C.6c** TEST #6 The recovery of unstable behavior
Source Fluid Temperature vs. Mass Flow Rate,
conditions as in Figure C.6a.
- Figure C.6d** TEST #6 The recovery of unstable behavior
Sink Fluid Temperature vs. Mass Flow Rate, conditions as in Figure C.6a.
- Figure C.7a** TEST #7 The recovery of unstable behavior starting from (almost) rest
using **RELAP5/MOD3.0**
Mass Flow Rates in Legs and TDV junction, 90 nodes per leg,
(Length of Components = 0.11m, Heated Length = 0.1m,
Initial Mass Flow Rate = 0.001Kg/s)
- Figure C.7b** TEST #7 The recovery of unstable behavior starting from (almost) rest
Mass Flow Rate in Ascending Leg, 90 nodes per leg,
(Length of Components = 0.11m, Heated Length = 0.1m,
Initial Mass Flow Rate = 0.001Kg/s)
- Figure C.7c** TEST #7 The recovery of unstable behavior starting from (almost) rest
Fluid Temperatures at Source, Ascending Leg Cell 5, Sink and
Descending Leg Cell 5, conditions as in Figure C.7a.
- Figure C.7d** TEST #7 The recovery of unstable behavior starting from (almost) rest
Fluid Temperatures at Source and Sink, conditions as in Figure C.7a.
- Figure C.7e** TEST #7 The recovery of unstable behavior starting from (almost) rest
Source Fluid Temperature vs. Mass Flow Rate,
conditions as in Figure C.7a.
- Figure C.7f** TEST #7 The recovery of unstable behavior starting from (almost) rest
Sink Fluid Temperature vs. Mass Flow Rate, conditions as in Figure C.7a.
- Figure C.8.a** TEST #14 Search for Neutral Stability using **RELAP5/MOD3.0**
Mass Flow Rates in Ascending Leg and toward TDV, 37 nodes per leg,
(Length of Components = 0.11m, Heated Length = 0.1m,
Initial Mass Flow Rate = 0.001Kg/s)
- Figure C.8b** TEST #14 Search for Neutral Stability
conditions as in TEST #7
Fluid Temperatures at Source and Sink conditions as in Figure C.8a.

- Figure C.8c** TEST #14 Search for Neutral Stability
Source Fluid Temperature vs. Mass Flow Rate,
conditions as in Figure C.8a.
- Figure C.8d** TEST #14 Search for Neutral Stability
Sink Fluid Temperature vs. Mass Flow Rate, conditions as in Figure C.8a.
- Figure C.9a** TEST #19 Sensitivity of results of TDV isolation using RELAP5/MOD3.0
Mass Flow Rates in Ascending Leg, 37 nodes per leg,
(Length of Components = 0.263m, Heated Length = 0.1m,
Initial Mass Flow Rate=0.001Kg/s)
- Figure C.9b** TEST #19 Sensitivity of results of TDV isolation at 3000s
Flow rates to/from TDV, Test #9 with valve left open up to 9000s
Conditions as in Figure C9.a
- Figure C.9c** TEST #19 Sensitivity of results of TDV isolation at 3000s
Flow rates in Ascending Leg, Comparison of Tests #9 and #19
Conditions as in Figure C9.a
- Figure C.10** TEST #14 Search for Neutral Stability, conditions as in TEST #7
Mass Flow Rates in Ascending Leg using RELAP5/MOD3.0 and MOD2,
90 nodes per leg, Length of Components =0.11m, Heated Length = 0.1m,
Initial Mass Flow Rate = 0.001Kg/s

EXECUTIVE SUMMARY

Theoretical results dealing with natural circulation in single-phase in a loop formed by two parallel adiabatic tubes with a point heat sink at the top and a point heat source at the bottom are considered. They are used to test the capability of the RELAP5 series of codes to predict instabilities in these flows.

The solution was useful to test two basic numerical properties of the RELAP5 code, namely:

- a) Convergence to steady state flow-rate using a "lumped parameter" approximation to both the heat source and sink
- b) The effect of nodalization to numerically damp the instabilities.

It was shown that, using a single volume to lump the heat source and sink, it was not possible to reach convergence to steady state flow rate when the heated (cooled) length was diminished simultaneously keeping constant the total heat transferred to (and removed from) the fluid. This is due to the numerical properties of the finite-differences scheme used.

Concerning the effect of nodalization on the damping of instabilities, it was shown that "reasonably fine" nodalizations led, as expected, to the damping of the solution. However, the search for convergence of numerical and theoretical results was successful, showing the nearly chaotic behavior of the system. This search led to refined nodalizations. The results obtained have also been verified by the use of simple, ad hoc codes.

A procedure to assess the effects of nodalizations on the prediction of instabilities threshold using RELAP5/MOD3.x is proposed. This procedure is based on the experience gained with simpler codes used and is outlined in this report.

ACKNOWLEDGEMENTS

Work was started while one of the authors (J.C.F.) was on leave at the Università di Pisa at the end of 1994. The partial support of the International Atomic Energy Agency for his stay is gratefully acknowledged. The kind and friendly collaboration of the Staff of the Dipartimento Costruzioni Meccaniche e Nucleari is also gratefully recognized. Subsequent work has been done in both institutions. The results are the product of a fruitful, non-formal collaboration. The CAMP provided the intellectual frame for this continued effort.

NOMENCLATURE

Roman Letters

A	Area	[m ²]
a, b	Coefficients of the friction law	[-]
C	Courant number	[-]
C _p	Specific heat at constant pressure	[J/(m ³ K)]
D	Diameter	[m]
$\mathcal{D}(q)$	Diffusion coefficient	[-]
F _{nod} (q)	Source-sink heat transfer multiplier for the nodal solution	[-]
f	Friction factor	[-]
<u>A</u>	Amplification matrix	
g	Gravity	[m/s ²]
H	Heat transfer coefficient	[W/(m ² K)]
<u>J</u>	Jacobian matrix	
L	Loop length	
N	Number of nodes	
Q	Volumetric flow rate	[m ³ /s]
q	Dimensionless volumetric flow rate	[-]
R	Friction parameter (from Welander [1])	[1/s]
Re	Reynolds number based on pipe diameter	[-]
S	Axial coordinate along the loop	[m]
T	Fluid temperature	
T _s	Fluid temperature in the source	
t	Time	
z	Eigenvalue	

Greek Letters

α	Buoyancy parameter in dimensionless momentum equation	[-]
β	Isobaric expansion coefficient	[-]
ε	Friction parameter in dimensionless momentum equation	[-]
μ	Fluid dynamic viscosity	[kg/(ms)]
ν	Fluid kinematic viscosity	[m ² /s]
$\rho(\underline{A})$	Spectral radius	[-]

Subscripts

ss	steady-state value
w	wall
Wel	Welander
0	reference or initial value

Superscripts

n	Value at time level n
n+1	Value at time level n+1

ss Steady-state value

Abbreviations

US NRC	United States Nuclear Regulatory Commission
UP	University of Pisa
FTUS	Forward Time Upwind Space
ODE	Ordinary Differential Equation
PDE	Partial Differential Equation

I. INTRODUCTION

The assessment of best estimate, nuclear safety codes is a very important stage in their development, including several steps. These steps are embedded in some accepted procedures like the U.S. NRC Code Scaling, Applicability and Uncertainty verification methodology [2] or the UP Uncertainty Methodology based on Accuracy Extrapolation [3]. Both specify the verification of the influence of the numerical methods implemented in such codes on the results obtained as a part of the applicability step. Then, defining suitable analytic tests and using them to set the conditions to satisfy in order to get meaningful results, is an important part of the verification stage.

The interest of the present work deals with the RELAP5/MOD3.x [4] series of codes. An important contribution to this subject has been contributed by Wulff et al. [5]. It is one of the rare examples of reports dealing with the effects of discretization errors in the response of thermal-hydraulic system codes in plant behavior analysis. In a more limited context and despite of its restrictions, the problem of natural circulation in single-phase flows is quite common in many situations of interest in the nuclear industry. The removal of decay heat in intact loops after pump shutdown is only one example of the possible scenarios.

In this report the results of Welander [1] are revisited. These results deal with the natural circulation in a very simple situation, namely: flow driven by buoyancy in a loop constructed with parallel, adiabatic, vertical tubes. The loop has a point heat source in its bottom and a point heat sink in its top. The mode of heat transfer is such that the product of the heat transfer coefficient in the heated length times the heated length is kept constant when the heated length tends to zero. This defines the heating rate. The same concept is applied in the heat sink. In this way, the physically finite heat source (sink) becomes a point.

Welander [1] performed his analysis only for laminar flow. However, his results may be generalized to consider turbulent flow. Chen [6], among many other authors, performed such analysis for a more general loop considering heated (cooled) horizontal tubes of finite length. In this report the analysis in [1] is generalized in order to keep strictly the same hypotheses of the original derivation. The analysis is included as APPENDIX A to this report. The results of such analysis are applied to verify whether or not the RELAP5 results may converge when the lengths of the source and sink are varied accordingly to the above-mentioned criterion. APPENDIX B to this report gives an algebraic justification for non-convergence of the upwind space approximation for the heat transfer. Having defined the theoretical stability map, an unstable flow condition is defined to check the effect of the nodalization on the appearance of oscillations. In this way it is possible to define the limits of applicability of a coarse nodalization. It is important to point out from the very beginning that it is possible to get convergence of the predicted results to the expected oscillatory analytical results. However, a nodalization much more detailed than the usually accepted for stable flows must be used.

These aspects may be also analyzed far more easily using *ad hoc* codes of similar numerical properties. Then some results are shown using in-house

developed codes. These results serve to illustrate a procedure that could be implemented using the RELAP5 numerical approximation. This may be of importance to quantify the effects of the nodalization in the damping of perturbations in unstable (or marginally stable) systems.

In what follows the geometry of the loop and the equations that specify the theoretical problem are briefly discussed. They include their generalization to consider turbulent flow and the analysis of the lumped parameter approximation for the point heat source and sink. The theoretical implications of the latter, from the numerical point of view, are discussed. Then, results obtained using the RELAP5/MOD3 and comparisons with RELAP5/MOD2 are presented, confirming the theoretical hypotheses. The discussion of the results and the conclusions close the report.

II. THEORETICAL ANALYSIS

Figure 1a,b shows the geometry of this simple hydraulic system, adapted from [1]. It is a schematic representation of the loop, appropriate for its discretization following the RELAP5 code specifications. These are shown in Figure 1c,d. The vertical legs are adiabatic, smooth, circular tubes of length $L/2$ and diameter D . The length of both the heat source and the heat sink is S . The cross section of the tubes is A . When S tends to zero, the heat transfer from/to the heat source/sink (shaded in Figure 1c,d) is increased to keep constant the total heat transferred. The role of the volume denoted as TDV (a time dependent volume) will be clarified later. This element, of course, is not present in the analysis in reference [1].

To deduce the governing equations, the validity of the Boussinesq expansion of the fluid density in terms of temperature will be assumed. The friction will be computed from the Poiseuille law for laminar flow and from the Blasius law for turbulent flow.

Then, the governing equations are:

i) The momentum equation integrated along the loop:

$$\frac{dq}{dt} + \frac{a \cdot R}{16} \left(\frac{D}{v \cdot A} \right)^{1-\theta} \cdot q^{2-\theta} = \frac{\beta g A}{L} \int_0^{L/2} (T - T_0) \cdot ds \quad (1)$$

In Eq. (1), the anti-symmetry of the system has been considered.

ii) The energy equation, expressed in terms of temperature:

$$C_p \left[\frac{\partial T}{\partial t} + \frac{q}{A} \frac{\partial T}{\partial s} \right] = \begin{cases} \pi D S H (T_F - T) \\ 0 \end{cases} \quad (2)$$

In equation (2), the first equality holds at the source/sink, and the second indicates the adiabatic walls of the tubes.

iii) The heat balance at the point heat source/sink:

$$T_s - T_{sI} = (T_F - T_{sI}) \cdot \left[1 - e^{-\left(\frac{\gamma H S}{q}\right)} \right], \quad q > 0 \quad (3)$$

In the previous equations, written in dimensional form, q is the volumetric flow-rate, T is the fluid temperature, H is the heat transfer coefficient, ν is the fluid kinematic viscosity, θ is a coefficient equal to 1 for laminar flow and to 1/4 for turbulent flow (the exponent in the Blasius friction law), a is the coefficient in the friction law: it equals 16 for laminar flow and 0.079 for turbulent flow, β is the volumetric expansion coefficient of the fluid and g is the acceleration of the gravity. The sub-index SI means a condition evaluated at the input of the source, sub-index S means a condition prevailing at the source and sub-index F indicates a temperature evaluated at the source wall. In Eq. (1) there is a derived coefficient R and, in Eq. (3), it is γ . Their definitions are:

$$R = 32 \frac{\nu}{D^2} \quad \text{and:} \quad \gamma = \frac{\pi D}{C_p} \quad (4)$$

The definition of R takes into account the total frictional force that must exist in the loop to make the results in [1] coincident with those given considering the Poiseuille law. The effect of the assumptions regarding the friction law will be discussed later.

Setting the temperature at the heat source wall at ΔT degrees above the average loop temperature and considering steady state, then, using Equations (1-3), the flow-rate may be obtained from the following implicit equation:

$$2\delta \cdot q_{ss}^{2-\theta} = \Delta T + \delta \cdot q_{ss}^{2-\theta} \cdot \left[1 - e^{-\left(\frac{\gamma H S}{q_{ss}}\right)} \right] \quad (5)$$

where δ is defined by:

$$\delta = \frac{2a \left(\frac{D}{A\nu} \right)^{1-\theta} \frac{\nu}{D^2} L}{\beta g A L}$$

The solution of Eq. (5) must be iterated if the flow-rate does not coincide with the postulated flow regime. This is not the case when the Reynolds number is adopted as the dependent variable, instead of flow rate. In non-dimensional terms,

Eq. (5) specifies the relation between flow-rate and steady state temperature in the loop, namely:

$$\frac{2 \cdot Q_{SS}^{2-\theta}}{\frac{\alpha}{\varepsilon} + Q_{SS}^{2-\theta}} = 1 - e^{-1/Q_{SS}} \quad (6)$$

where:

$$Q = \frac{q}{(KS)A} ; \quad \Theta = \frac{T}{\Delta T} ; \quad \alpha = \frac{\beta g \Delta T L}{2(KS)^2} ; \quad K = \frac{\pi D H}{C_p A} ;$$

$$\varepsilon = \frac{a}{16} \left(\frac{DKS}{v} \right)^{1-\theta} \cdot \frac{RL}{2(KS)} \quad \text{and} \quad \varepsilon_{Wei} = \frac{\varepsilon}{\frac{a}{16} \left(\frac{DKS}{v} \right)^{1-\theta}}$$

When $\theta=1$ and $a=16$ the previous equations reduce to the ones in [1]. The linearized analysis of the stability of the steady state equations may be performed in similar terms as in [1]. Now, ε shows the influence of the Reynolds number in the system through the friction law coefficients.

Let us now consider a "lumped parameter" approach to model the heat transfer from the heat source toward the fluid. Note that the anti-symmetrical situation must be considered for the sink. Details of the derivation may be found in APPENDIX B. The steady state energy equation, evaluated at the source, gives the value of the temperature in the fluid. For this purpose the steady state energy equation and an upwind approximation are used.

Then, the value for the fluid steady state temperature at the source is:

$$\Theta_{SS} = \frac{1}{1 + 2Q_{SS}} \quad (7)$$

Note that Q_{SS} is only a function of the quotient α/ε that is a non-dimensional parameter depending on the physical parameters of the system and on the product (KS) that must be kept constant, it may be concluded that the results obtained applying the r.h.s. of Eq. (2) as it stands will not change using a smaller node length. For example: if $\alpha/\varepsilon=2$ and $\theta=1$ (laminar flow), then $Q_{SS}=0.958$ and $\Theta_{SS}=0.479$ from the theory. The value, as computed from Eq. (7) is $\Theta_{SS}=0.342$. There is only one way to obtain the correct steady state value of Θ_{SS} , it is to get the analytical solution of Eq. (3) averaging over the length S . Following this procedure and using the upwind approximation for the advective term, the expression for Θ_{SS} is:

$$\Theta_{SS} = \frac{F}{2-F} \quad , \quad \text{where: } F = 1 - e^{-1/Q_{SS}}$$

The value of Θ_{SS} computed with this expression is coincident with the theoretical value.

III. NUMERICAL RESULTS

Three versions of RELAP5 [4] have been applied in the present work, namely: MOD2, MOD3.0, and MOD3.1. Due to the simplicity of the physical problem considered (single-phase flow, constant wall temperature and heat transfer coefficient), no relevant differences in the behavior of the different versions was noted in relation to the capabilities in predicting the stability threshold. Then, the results obtained will be reported specifying the code version just for the sake of completeness. The tests involving the MOD2 version have been also considered to check alternative, more detailed nodalizations to the heat/sink volumes in the early stages of this work.

The basic nodalization adopted in the analysis is reported in Figure 1d. It consists of two BRANCH components (100 and 130) introduced to simulate the lower heating and the upper cooling devices. A very thin structure is connected to each of them, with imposed external temperature, in order to simulate the actual boundary conditions consisting in an imposed internal wall temperature. The two BRANCH components are joined with two PIPE components (110 and 120), simulating respectively the ascending and the descending legs. A SINGLJUN (300) and a TMDPVOL (400) have been included to compensate for the expansion or contraction of the fluid volume inside the system. However, specific calculation tests have shown that the dynamic behavior of the system is negligibly affected by the presence of these components.

The application of the system code to Welander's problem was concerned with a physical system having the following main characteristics (see other details in Table 1):

- pipe inner diameter: 0.1 m;
- length of the legs: 10 m;
- length of the heating and cooling sections: 0.1 m to 1 m;
- overall loop length: 20 m + 2 x heating section length;
- heating surface temperature: 30 °C;
- cooling surface temperature: 20 °C;
- heating and cooling surface heat transfer coefficient: 20000 W/(m²K);
- system pressure: 10⁵ Pa;
- pipe surface roughness: 10⁻⁷ m.

Appendix C reports the list of the calculation cases considered, together with the plots of the related results. Most of the cases were run with a time step of 0.5 s. Various heating lengths and number of nodes were used to test the convergence of RELAP5/MOD3.x to the theoretical solution.

The topics of main interest were:

1. the treatment of the source and the sink, which in the upwind scheme adopted by the code cannot be correctly simulated using a single node, since the exponential trend of the fluid temperature inside the heating and the cooling sections cannot be adequately accounted for, and
2. the effect of truncation error related to the discretization of the legs by a finite number of nodes: this is known to introduce spurious dissipative effects that result in damping the oscillations.
3. the effect of Courant number on scheme numerical phase lags, which may lead to over prediction of instability for a given nodalization.

The flow was started at very low flow-rate and began to grow as time elapsed. In damped calculations, the temperature in the loop increased up to the point in which it reached the average value as given by their theoretical value, the latter depending on the adopted criteria for the source/sink lumping.

The main conclusions coming from the analysis of the obtained results were the following:

- The steady-state conditions predicted by Welander cannot be achieved, unless an appropriate source heat transfer multiplier is included in the code.
- For a given time-step, it is possible to predict both stable and unstable conditions, depending on the number of nodes adopted to discretize the legs.

The analysis to follow applies to the first conclusion. For these calculations the following spatial discretization have been considered: 10 nodes in each leg ($\Delta x = 1$ m) and $S = 1.0, 0.5$ and 0.1 m (correspondingly, the values for H were: 2000, 4000 and 20000 W/ m².K). It must be pointed out that the flow was unstable with these parameters. The code was RELA5/MOD3.0. As expected, the value of the steady state temperature was almost the same, with small differences that were due to the different total friction in the loop. The effect of the TDV volume was not important as will be discussed later. Naturally, oscillations in the transition to steady state were present. The behavior of the system may be observed in Figure 2 for the fluid temperature at both the heat source and sink. The results obtained confirmed the results predicted by the theoretical analysis. Then, to improve convergence toward theoretical values, an average, lumped heat source must be used, as suggested previously.

Let us now consider the problem of convergence of the code results to the expected unstable results. To do this, let us suppose that we do not know that the flow is unstable and proceed as CSAU, UMAE (and engineering judgment) indicate: look for convergence of computed results. For this purpose the nodalization considering $S = 0.1$ m and 20000 W/ m².K was used. The number of nodes in each leg was varied accordingly up to the point in which the expected chaotic behavior was obtained. The latter made its first appearance when the number of nodes per leg was increased from 25 to 50. Nearly neutral oscillations in flow-rate were observed for 37 nodes per leg.

Figure 3 shows the time variation of flow-rate using 90 nodes per leg and 0.001 Kg/s of starting flow-rate. As may be observed the flow is oscillatory, switching from positive to negative values after some cycles of oscillation. Fluid temperature varies correspondingly.

The system behavior may be observed more clearly when the temperature in the sink is plotted versus flow-rate in the loop. Figure 4 is a clear indication of the chaotic behavior of the system.

Figure 5 presents results of the calculations, performed with 40 and 60 volumes per leg, still using the semi-implicit numerical method of the code. They were started close to steady-state conditions. The values of α and ϵ corresponding to the considered physical problem are around 339 and 2.3 respectively, identifying a physically unstable system (see Figure A.3), and it may be found that the time-step adopted in the calculation, $\Delta\tau = 0.05$ s, roughly corresponds to a dimensionless time-step $\Delta t = 10^{-4}$. It can be noted that, with the two numbers of nodes adopted, stable and unstable conditions are predicted, owing to the different damping introduced by truncation error.

Simply closing the connecting junction in the middle of an unstable transient controlled the effect of the TDV. The effect of this action on the flow variables was negligible and could not be recorded. Also, the same results have been obtained running the same cases with RELAP5/MOD2. The results were also verified running a small, ad hoc code using an integrated equation approach for the momentum equation and a fully up-wind, explicit approximation for the energy equation. The equivalent, length-averaged heat source/sink approach was used for lumping, what allowed obtaining of the exact steady state flow-rate value when possible. The same numerical behavior was observed.

In what follows, a more detailed numerical analysis will be outlined, making reference to the FTUS approximation. This numerical scheme is quite similar to the one used in RELAP5. Then the algebraic equations expressing the energy balance are the following:

- $q \geq 0$

$$\begin{aligned}\Theta_i^{n+1} &= (1 - C) \Theta_i^n + C \Theta_{i-1}^n && (i=2, \dots, N-1) \\ \Theta_N^{n+1} &= \left(1 - C - \frac{\Delta t}{\Delta S} F_{\text{nod}}(Q^n)\right) \Theta_N^n + C \Theta_{N-1}^n - \frac{\Delta t}{\Delta S} F_{\text{nod}}(Q^n) \\ \Theta_1^{n+1} &= -\Theta_N^{n+1}\end{aligned}\tag{8}$$

- $q < 0$

$$\begin{aligned}\Theta_i^{n+1} &= (1 + C) \Theta_i^n - C \Theta_{i+1}^n && (i=2, \dots, N-1) \\ \Theta_1^{n+1} &= \left(1 + C - \frac{\Delta t}{\Delta S} F_{\text{nod}}(Q^n)\right) \Theta_1^n - C \Theta_2^n + \frac{\Delta t}{\Delta S} F_{\text{nod}}(Q^n)\end{aligned}\tag{9}$$

$$\Theta_N^{n+1} = -\Theta_1^{n+1}$$

where C is the Courant number:

$$C = \frac{Q^n \cdot \Delta t}{\Delta s} \quad (10)$$

and

$$\Delta s = \frac{1}{N-1} \quad (11)$$

with N being the number of nodes. The function $F_{nod}(q)$ is a source-sink heat transfer multiplier, similar to the one adopted for the nodal expansion, introduced in order to calculate the steady-state conditions in coincidence with the exact solution.

The momentum equation is discretized in time as follows:

$$Q^{n+1} = Q^n + \left(\frac{\alpha}{N-1} \sum_{i=1}^{N-1} \frac{\Theta_i^n + \Theta_{i+1}^n}{2} - \varepsilon (Q^n)^{2-\theta} \right) \Delta t \quad (12)$$

The steady-state conditions calculated by the method are:

$$\Theta_{SS,1} = \Theta_{SS,2} = \dots = \Theta_{SS,N-1} = -\Theta_{SS,N} = \Theta_{SS,leg}$$

$$\Theta_{SS,leg} = \frac{F_{nod}(Q_{SS})}{2Q_{SS} + F_{nod}(Q_{SS})} \quad (13)$$

where:

$$F_{nod}(Q_{SS}) = Q_{SS} (1 - e^{-1/Q_{SS}}) / e^{-1/Q_{SS}} \quad (14)$$

Thus, the result is:

$$Q_{SS} = \frac{\alpha}{2\nu} \frac{1 - e^{-1/Q_{SS}}}{q^{1/Q_{SS}}} \frac{2}{1 + e^{-1/Q_{SS}}} \frac{N-2}{N-1} \quad (15)$$

It can be easily shown that for $N \rightarrow \infty$ the above equation becomes coincident with the exact expression given by Equation (5).

The assessment of the effects of nodalizations on the onset of instabilities will be performed using the previous expressions. However, as will be mentioned later, some other methodologies have been also considered. This approach can be considered the numerical analogue of the classical linear stability analysis of PDEs. The main reasoning behind the methodology is shortly summarized in what follows. A finite-difference numerical method for a time-marching problem can be written as an algebraic η -vector equation relating the η values of the unknown function at the n -Th. and $(n+1)$ -Th. time level (\underline{y}^n and \underline{y}^{n+1}), grid

parameters (in the present case, Δs and Δt) and physical parameters (α , ϵ). This algebraic equation represents the discretized form of the original PDEs together with the related boundary conditions. In our specific case for the above-described numerical methods it is:

$$\underline{E}(\underline{y}^n, \underline{y}^{n+1}, \Delta t, \Delta s, \alpha, \epsilon) = 0 \quad (16)$$

It will be now shown that:

- Studying stability of steady-state solutions of a mathematical problem is capable of clearly pointing out the effect of truncation error brought about by the nodalization.
- Care must be taken in avoiding numerical instabilities or in recognising them in the obtained stability maps.

The vector function \underline{E} is generally non-linear. Therefore, determining the steady state conditions (i.e., the fixed points) may require the iterative solution of the equation:

$$\underline{E}(\underline{y}^n = \underline{y}_{ss}, \underline{y}^{n+1} = \underline{y}_{ss}, \Delta t, \Delta s, \alpha, \epsilon) = 0 \quad (17)$$

Once the fixed points have been determined, their stability can be studied through linearization by perturbation. Then, considering small deviations from the selected fixed point:

$$\underline{y}^n = \underline{y}^s + (\delta \underline{y})^n \quad \underline{y}^{n+1} = \underline{y}^s + (\delta \underline{y})^{n+1} \quad (18)$$

Substituting into Equation (16), second order terms can be neglected and Equation (17) can be used to reach the following relationship between perturbations at the n-Th. and at the (n+1)-Th. time levels:

$$(\delta \underline{y})^{n+1} = -(\underline{J}_{\underline{s}}^{n+1})^{-1} \cdot \underline{J}_{\underline{s}}^n \cdot (\delta \underline{y})^n \quad (19)$$

where $\underline{J}_{\underline{s}}^n$ and $\underline{J}_{\underline{s}}^{n+1}$ denote the Jacobian matrices of \underline{E} with respect to \underline{y}^n and \underline{y}^{n+1} respectively, calculated at the selected fixed point. It is clearly understood that the inverse of $\underline{J}_{\underline{s}}^{n+1}$ must exist for any meaningful time-marching numerical scheme; in particular, $\underline{J}_{\underline{s}}^{n+1}$ can be made equal to the identity matrix for explicit numerical methods and boundary conditions. It is then argued that stability can be discussed considering the eigenvalues of the matrix:

$$\underline{A} = -(\underline{J}_{\underline{s}}^{n+1})^{-1} \cdot \underline{J}_{\underline{s}}^n \quad (20)$$

As results assuming exponential growth or decay of perturbation vectors. In particular, given the spectral radius of the matrix, $\rho(\underline{A})$, it is useful to consider the quantity:

$$\Delta \rho = \rho(\underline{A}) - 1 \quad (21)$$

quantifying the *margin in excess to neutral stability*, which takes negative values for stable conditions and positive values for unstable ones. This quantity can be therefore used to find neutral stability conditions and to set up stability maps. Then, it is here preferred to calculate $\Delta \rho$ throughout a selected α - ϵ rectangular

domain, thus identifying with the aid of contour plots regions with a different degree of stability. This method is easier to implement in computer programs and has the advantage to provide a greater deal of information, at the price of a reasonable increase in computing effort.

Figure 6 reports the results obtained for the FTUS method with 30, 40, 50 and 100 nodes and $\Delta t=10^{-4}$. It can be noted that a very small unstable region is found within the addressed domain with 30 nodes, whereas increasing the detail of discretization unstable conditions are predicted for lower and lower values of α . This clearly explains the above-discussed behavior and shows the dramatic quantitative impact of truncation error on the prediction of stability.

Figure 7 illustrates the map for 100 nodes. It is interesting to compare the results obtained for the explicit upwind method with the results of a modal solution¹ with a second order term simulating numerical diffusion. With this aim, the diffusion coefficient is defined as:

$$\beta(Q) = \frac{|Q| \Delta s}{2} \left(1 - \frac{|Q| \Delta t}{\Delta s} \right) \quad (22)$$

as resulting from the analysis of truncation error for the FTUS method. Figure 8 shows the predicted flow rate variation with time. The diffusion coefficient was the one corresponding to 1000 nodes under the FTUS approximation. The number of modes considered in the modal expansion was 500. As may be observed, both approximations behave similarly. Exact coincidence is precluded by the non-linearity of the system and the approximate values given by expression (6). The latter fact is due to the use of the nominal, steady state value of Q used for its calculation. It may be shown that the predicted stability conditions are very similar for the nodal and the modal solution with equivalent dissipative effects and the agreement is improved by increasing the number of nodes. This confirms the overwhelming importance of the second order term alone in determining the overall truncation error effect on stability predictions. Figure 6 also shows the linear stability curve obtained by the modal solution with no diffusion ($\beta(Q)=0$). It shows, as expected, its close agreement with the stability curve obtained by the conventional linear stability analysis shown in APPENDIX A.

Finally, Figure 9 shows the stability maps for various 1st and 2nd order methods obtained with $\Delta t=10^{-4}$. It is clearly visible that 2nd order methods provide relatively very accurate predictions of the stability boundary. The changes observed in the maps increasing the number of nodes up to 100 are minimal, supporting the conclusion that in the present case the effect of truncation error on stability prediction is due almost exclusively to the second order dissipative term. The low Courant number used makes the FTUS results almost as diffusive as the ITUS ones.

¹ This consists in a modal expansion of the governing equations and boundary conditions (1-3) in terms of Fourier series of sinus and cosinus. Then, a coupled system of ODEs is obtained, which is free of spatial discretization error. Considering a reasonably high number of modes, a reference solution may be obtained. Then, the energy conservation equation may be generalized to consider a diffusive term, with diffusion depending on flow rate.

The analysis of the stability maps obtained with the FTUS method and $C=0.8$ or with second order methods and $\Delta t = 10^{-3}$, pointed out the appearance of regions of instability larger than those predicted by the reference modal solution. The possible reasons for this behavior were mainly two:

- An effect of truncation error at large time steps on the velocity of propagation of perturbations along the legs, related to the dispersive effects brought about by odd-order derivatives;
- The effect of the use of a large time step in momentum equation, giving rise to a general tendency to instability due to delayed feedback.

In what follows it will be shown that, although the first effect cannot be excluded, the second is the leading one, being responsible for the observed overprediction in the extent of the unstable region.

In all the cases considered (FTUS and 2nd order methods), the adopted discretization for the momentum equation implied that both the temperature integral along the loop and the friction term have been evaluated making use of old-time-level quantities. The results obtained making use of this form are shown in the Figures 15 and 16 below for both the FTUS method. It can be noted that in the case of FTUS with $C=0.8$, the overprediction of the extent of the stability region is remarkable. In the case of the MacCormack method with $\Delta t = 10^{-3}$, a slight discrepancy with the modal solution was also found.

The following approach was used to discriminate among the possible causes of this convergence “coming from outside” to the neutral curve:

- Considering a fully implicit linearized approximation of the friction term in the momentum equation: this approach did not lead to any improvement in the results. On the contrary, the degree of overprediction was larger, showing a more pronounced dependence on C .
- Evaluating the friction term and the temperature integral term on the basis of $(n+1)$ -Th time level values (It did not increase too much the computational effort):

Therefore, the following form of momentum equation results:

$$Q^{n+1} = Q^n + \left(\frac{\alpha}{N-1} \sum_{i=1}^{N-1} \frac{\Theta_i^{n+1} + \Theta_{i+1}^{n+1}}{2} - \varepsilon (Q^n)^{1-\theta} Q^{n+1} \right) \Delta t$$

Making use of this momentum equation in the FTUS scheme, the stability maps reported in Figures 17 and 18 were obtained. It can be noted that now no overestimate of the unstable region was obtained, showing the usual diffusive behavior.

The analysis above clearly demonstrates that of the two above envisaged reasons for overestimating instability, that related to the time discretization of the momentum equation is certainly dominant.

IV. CONCLUSIONS

The aforementioned calculations allowed arriving to the following conclusions:

i) The analytical results given in [1] are very useful to verify how large predictive codes, like the RELAP5 series of codes, treat lumped heat transfer structures. This may also be the case with other codes. Its proper understanding is very important when the lumping of heat exchanging structures is imperative. Imposing an appropriate criterion for the lumping avoid convergence errors in these cases.

ii) The effect of numerical diffusion may damp oscillations in a system, even under unstable flow conditions. Appropriate nodalization permits to recover the correct physical behavior. Looking for convergence of computed results is always rewarding in these situations.

iii) The methodology adopted in this work for setting up stability maps shows that a linear stability analysis based on numerical methods is effective in pointing out the effect of truncation error. Furthermore, if the appropriate nodalization detail and/or higher order schemes are adopted, it can even result as reliable as the usual frequency-domain techniques.

As shown by the obtained results, the methodology adopted in the present work is useful to quantify the effects of nodalization and time step choice (i.e. discretization errors) for system codes like RELAP5. This will be the subject of further research.

V. REFERENCES

- [1] Welander, P., On the Oscillatory Instability of a Differentially Heated Fluid Loop, J. of Fluid Mechanics, vol. 29, p 17-30, 1967.
- [2] Boyack, B.E. et al., Quantifying Reactor Safety Margins. Part 1: An Overview of the Code Scaling, Applicability and Uncertainty Evaluation Methodology, Nuclear Eng. and Design, vol. 119, p. 1-15, 1991.
- [3] D'Auria, F., Debrechin, N. and Galassi, G.M., Outline of the Uncertainty Methodology based on Accuracy Extrapolation, Nuclear Technology, vol. 109, p. 21-38, 1995.
- [4] Carlson, K.E. et al., RELAP5/MOD3 Code Manual Volume I: Code Structure, System Models and Solution Methods, NUREG/CR-5535, 1990.
- [5] Wulff, W., H.S. Cheng, A.N. Mallen and U.S. Rothagi, BWR Stability Analysis with the BNL Engineering Plant Analyzer, NUREG/CR 5816, 1992
- [6] Chen, K., On the oscillatory Instability of Closed-Loop Thermosyphons, ASME Trans., J. of Heat Transfer, vol. 107, p. 826-832, 1985

PARAMETER	VALUE
	SI Units
L	20.00
L/2	10.00
S	0.10
A	0.00785
D	0.10
T _{AV}	25.00
ΔT	5.00
T _w (at source)	30.00
T _w (at sink)	20.0
β	0.000255
ρ	997.00
C _p	4177.
μ	0.000864
ν	8.6660d-07
H	20000.
power to the source	2813.31
ss mass flow rate	0.717
ss vol. flow rate	.7193d-03
Reynolds number	10568.
ss (T-T _{AV})	0.522
D.K.S/ν	2216.7
U	0.09158
α	338.94
ε _{Wei}	1.4436
ε	2.3027
q _{ss}	4.7674
T _{ss}	0.1045

TABLE 1 Specification of a test problem

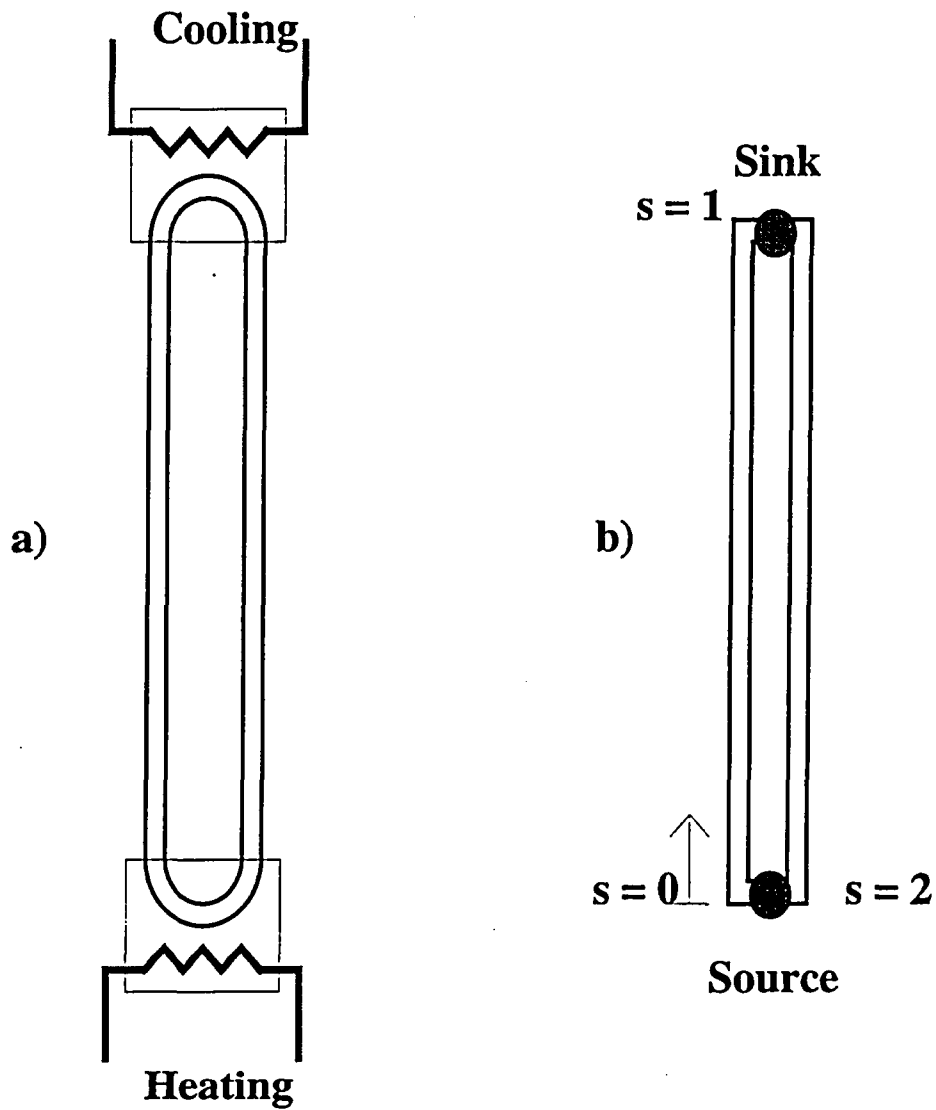


FIGURE 1a,b A schematic view of the natural circulation loop, adapted from [1]

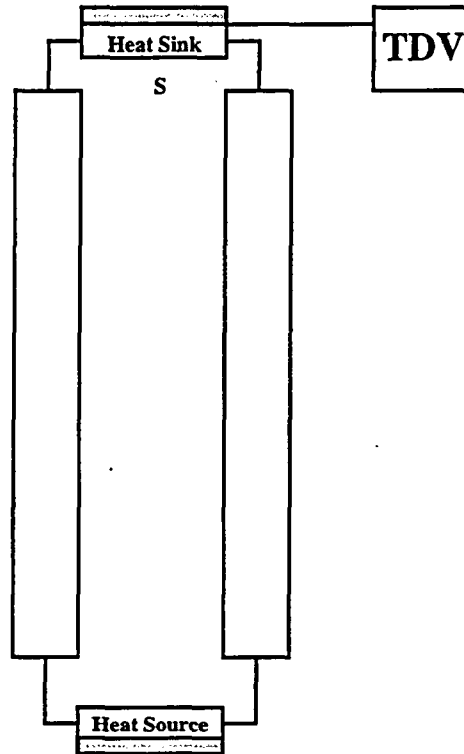


Figure 1c. The loop geometry in a RELAP5 like definition.

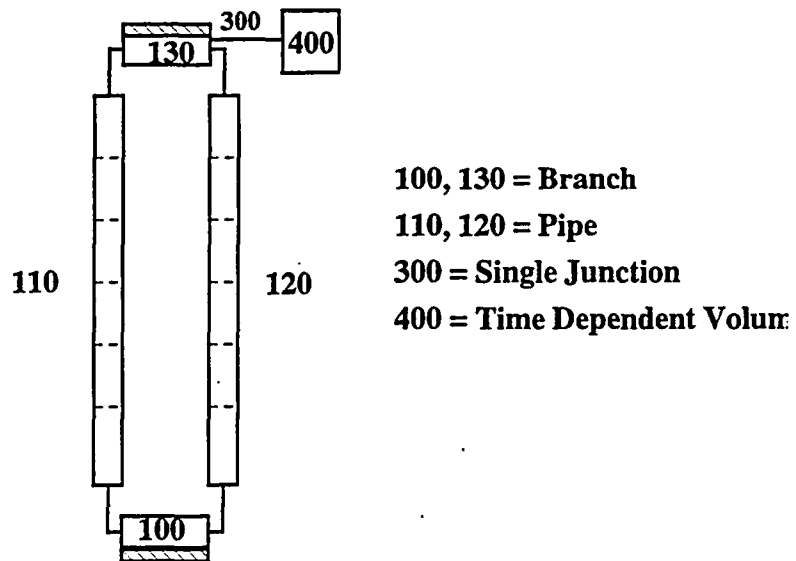


Figure 1d - RELAP5 code nodalization for the analysis of Welander's problem

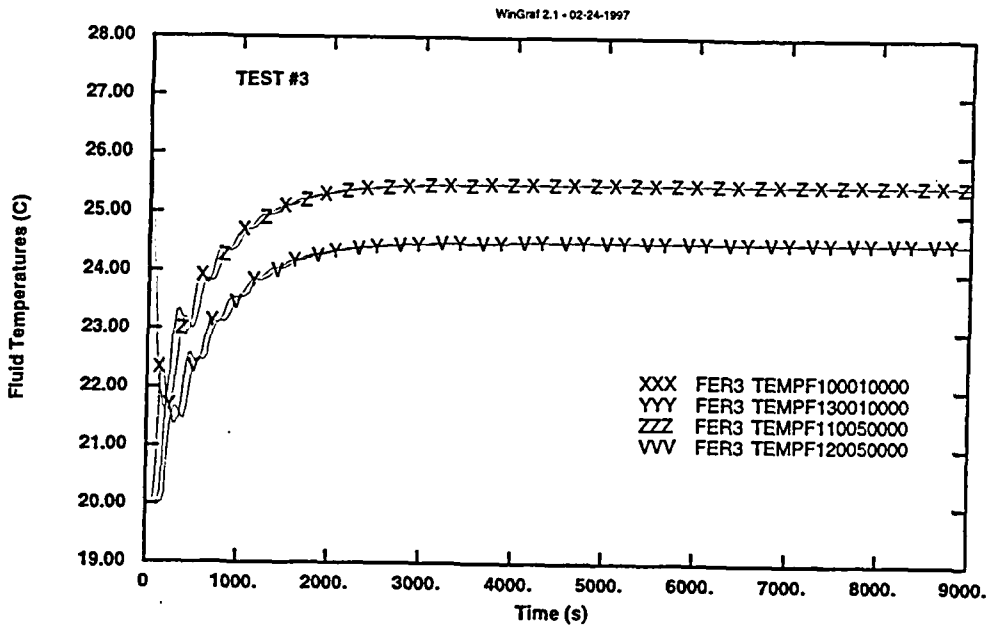


Fig. 2 The evolution of fluid temperature at the source and the sink vs. time using 10 nodes per leg and $S=0.1$ m, $\alpha = 339$, $\epsilon = 2.3$

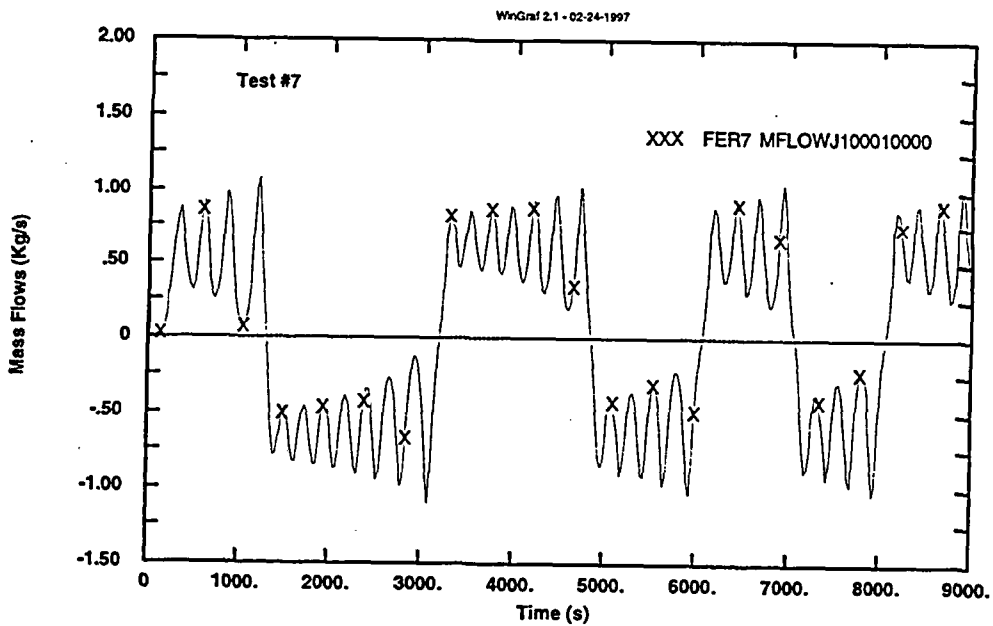


Fig. 3 The time variation of loop flow-rate.
Number of nodes per leg: 90, $S=0.1$ m, $\alpha = 339$, $\epsilon = 2.3$

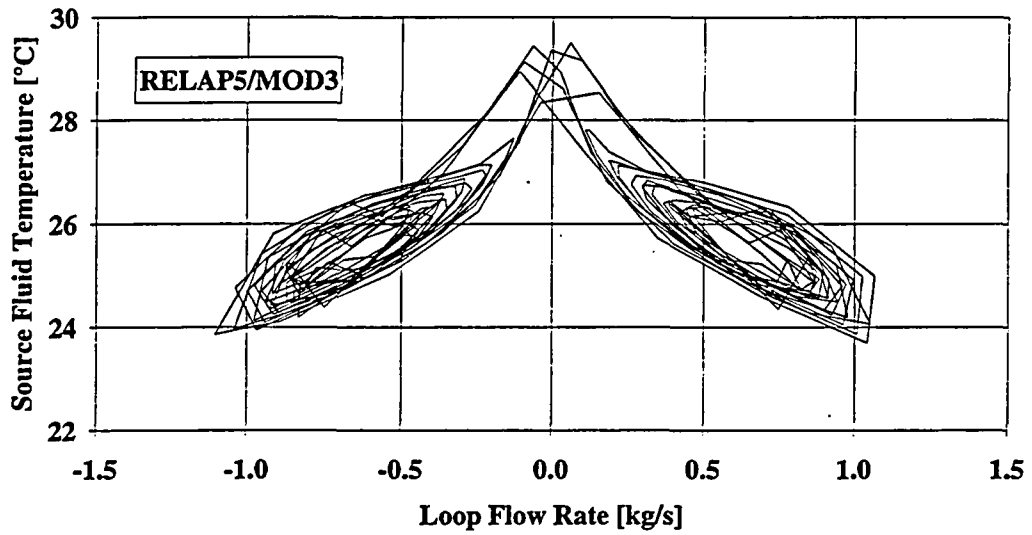


Figure 4 - Projection of the attractor in the phase space as calculated by RELAP5/MOD3 using 90 nodes per leg, $\alpha = 339$, $\varepsilon = 2.3$

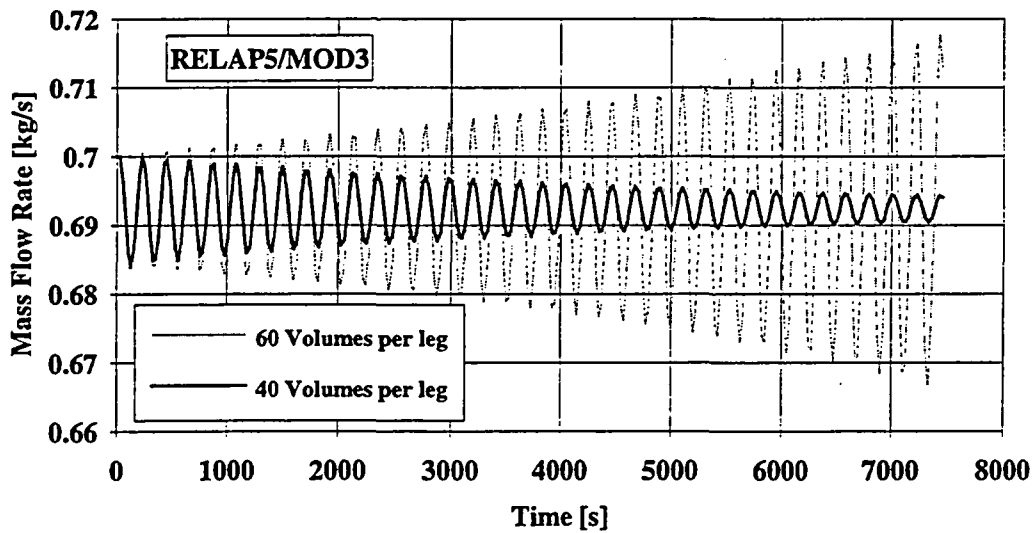


Figure 5 - RELAP5/MOD3 results for the dynamic behavior of a single-phase thermosyphon loop, $\alpha = 339$, $\varepsilon = 2.3$

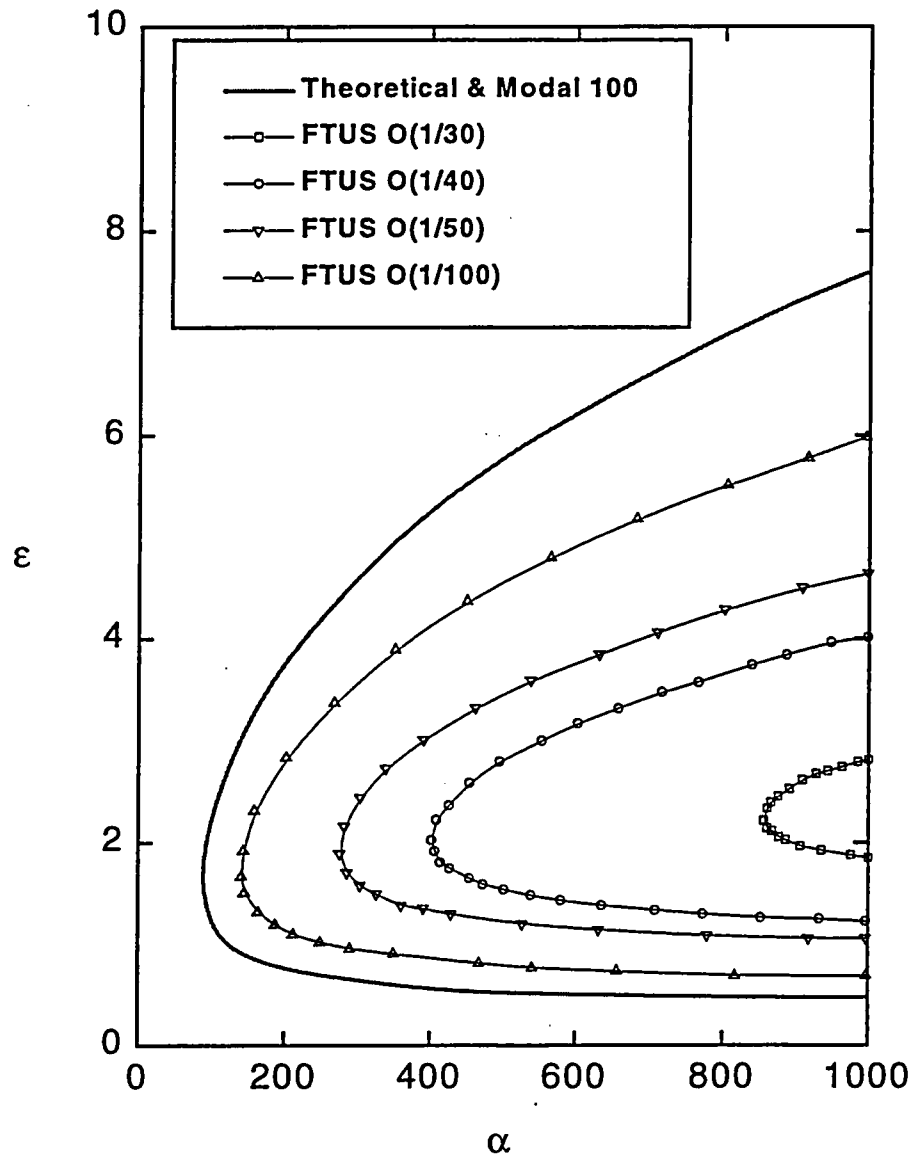


Figure 6 The effect of the number of nodes on the Neutral stability curve using the FTUS scheme.

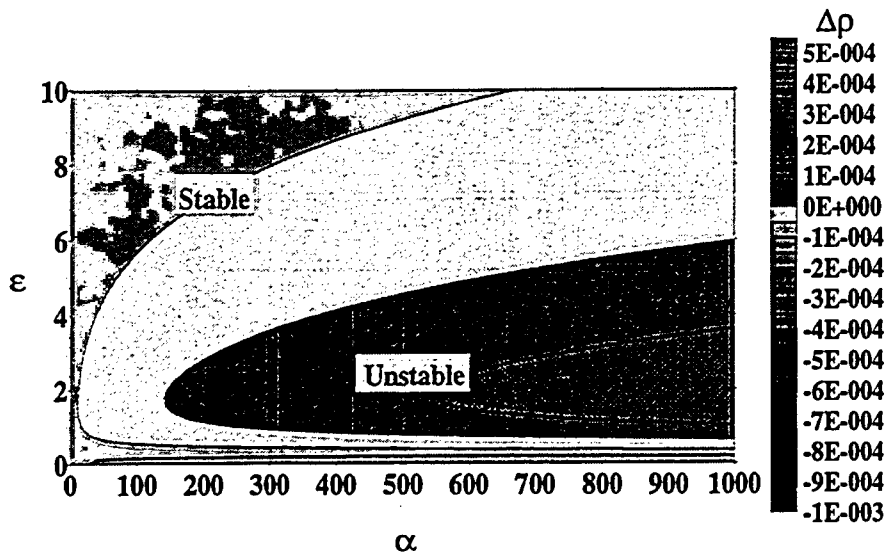


Figure 7 Stability map for the FTUS scheme, 100 nodes and $\Delta t=10^{-4}$

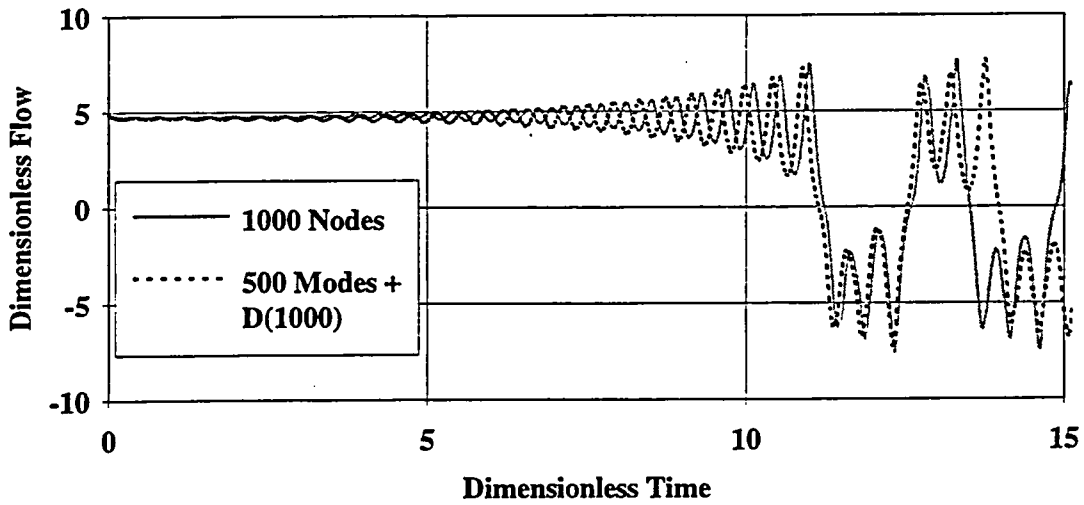


Figure 8 The flow rate for the FTUS scheme using 1000 nodes and its simulation using a modal expansion of 500 modes and expression (22)

NEUTRAL CURVES USING 100 NODES

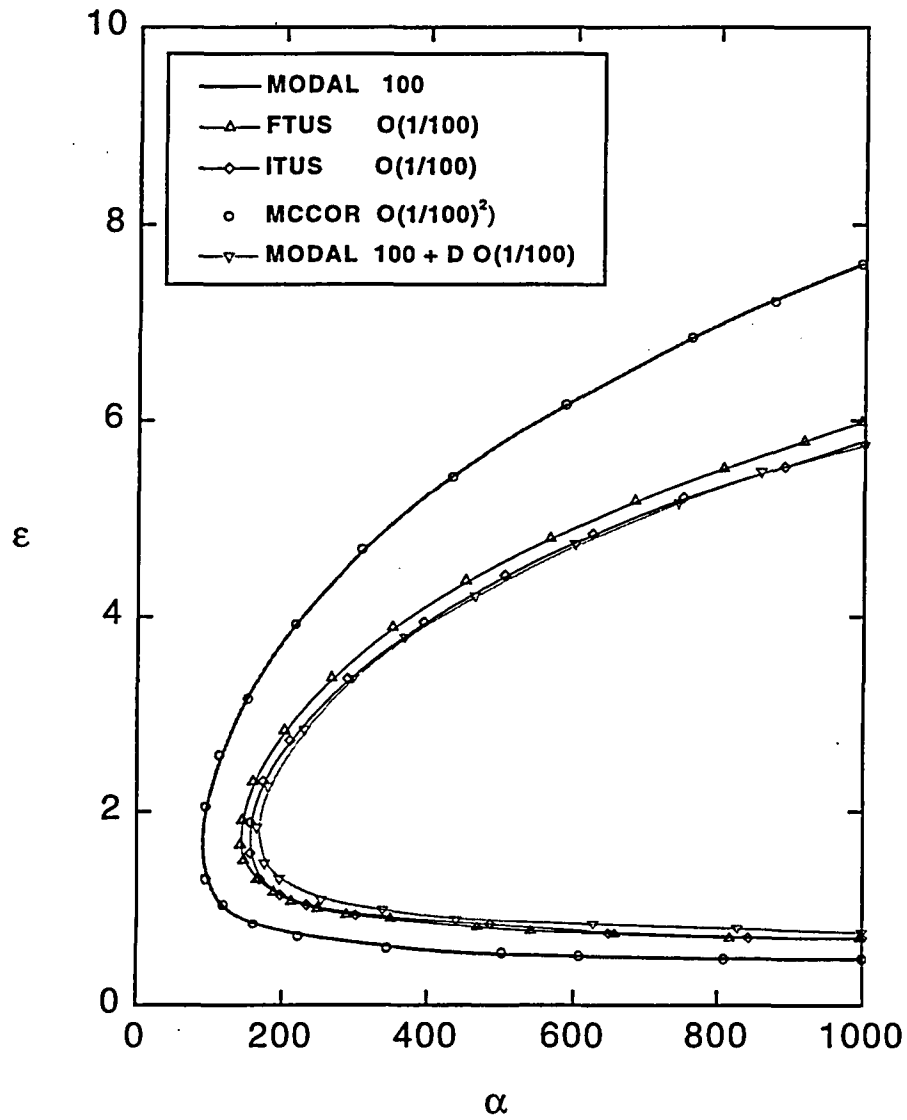


Figure 9 Comparison of the neutral curves obtained with different approximations (ITUS: implicit-time, Upwind-Space, MCCOR: Mac Cormack)

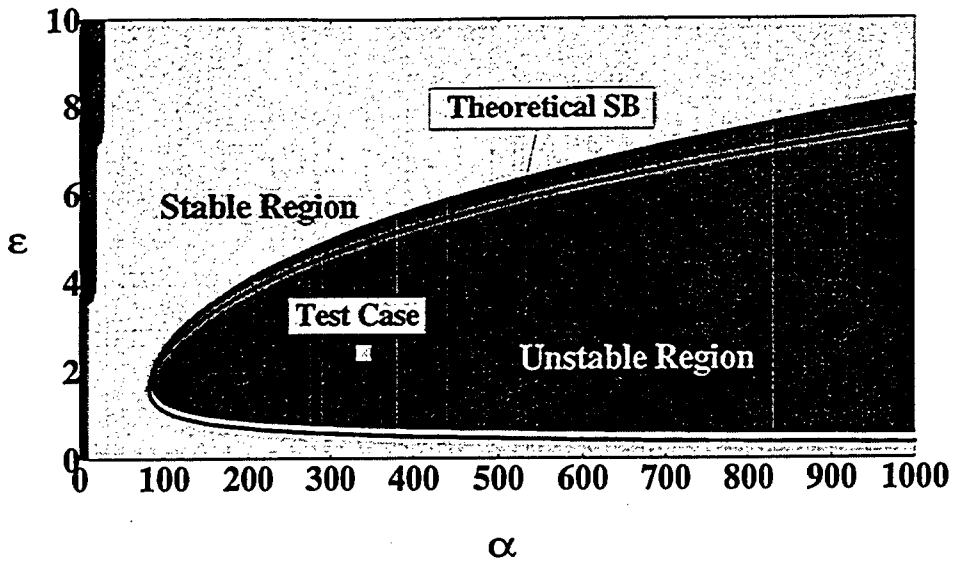


Figure 10 - FTUS scheme with $C=0.8$ and explicit momentum equation (30 nodes)

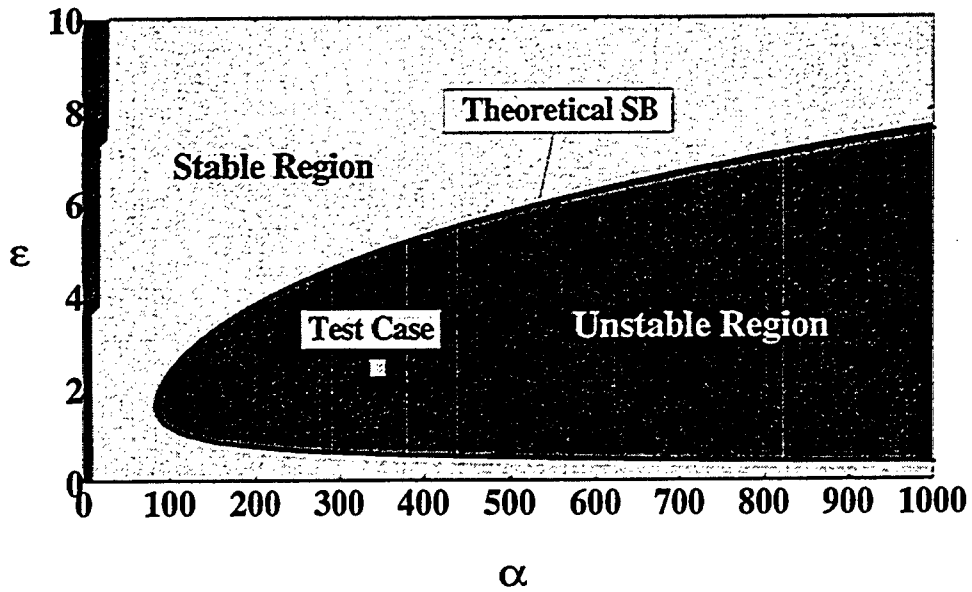


Figure 11 - FTUS scheme with $C=0.8$ and explicit momentum equation (100 nodes)

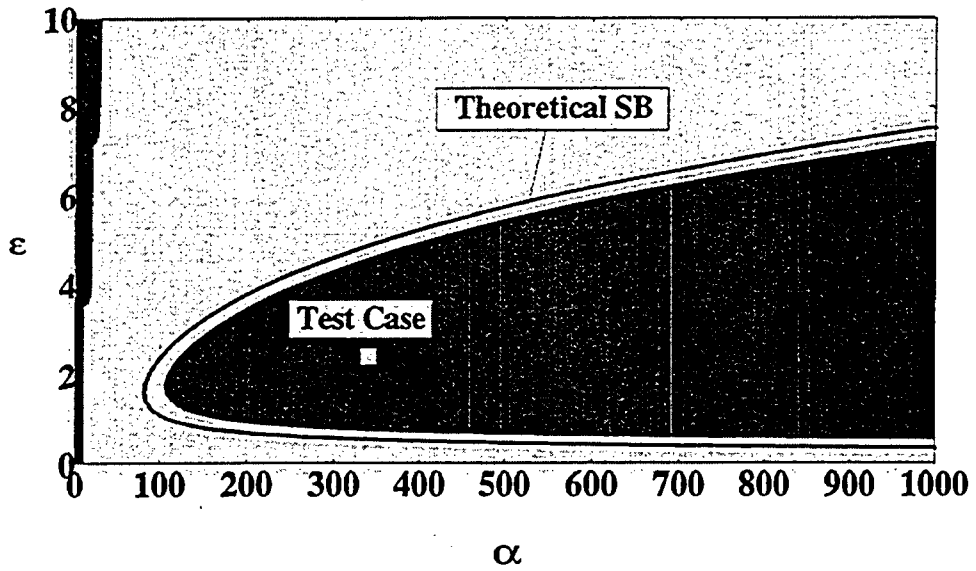


Figure 12 - FTUS scheme with $C=0.8$ and semi-implicit momentum equation (30 nodes)

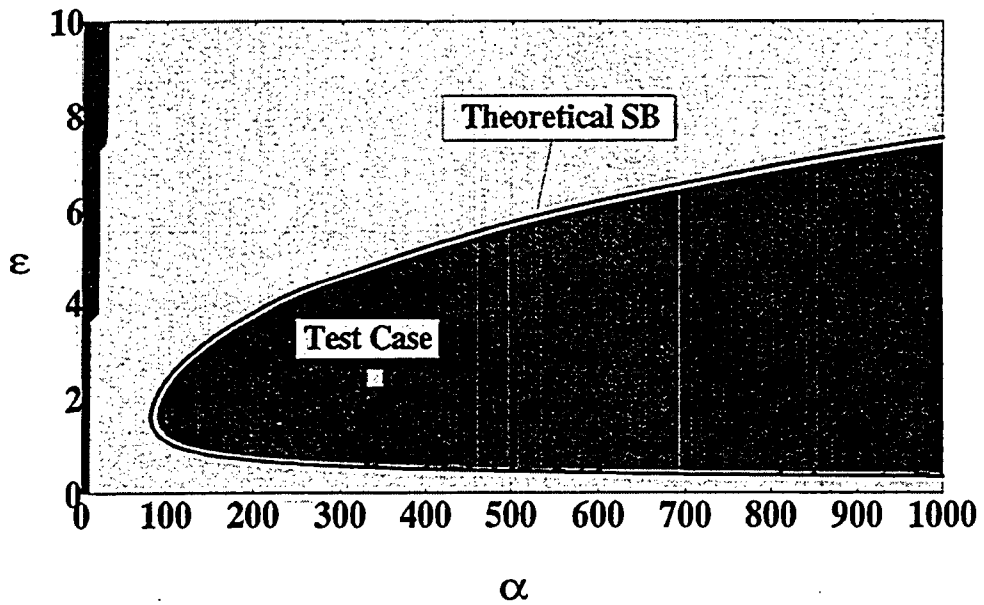


Figure 13 - FTUS scheme with $C=0.8$ and semi-implicit momentum equation (100 nodes)

APPENDIX A

THEORETICAL STABILITY ANALYSIS FOR TURBULENT NATURAL CIRCULATION IN A SIMPLE LOOP

In this APPENDIX, the analysis in [1] is generalized to consider turbulent flow, keeping strictly the same hypotheses of the original derivation. The results emerging from this analysis have been used in the main text to setup an unstable problem in such a way that a “reasonably” detailed discretization using the RELAP5 MOD 3.x [4] codes completely masked the physical situation, giving false stable solutions.

In what follows the geometry of the loop and the equations that specify the theoretical problem are briefly discussed. They include their generalization to consider turbulent flow. The neutral stability curves are obtained as a function of a new parameter, allowing the definition of a theoretical stability map.

The solution of equation (6) (see main text) must be iterated if the flow-rate does not coincide with the postulated flow regime. In non-dimensional terms equation (6) specifies the relation between flow-rate and steady-state temperature in the loop, namely:

$$T_{ss} \equiv \text{uniform in the leg} \tag{A.1-a}$$

$$2T_{ss} = (1 + T_{ss}) \left(1 - e^{-\frac{1}{q_{ss}}} \right) \tag{A.1-b}$$

$$\frac{2 \cdot q_{ss}^{2-\theta}}{\frac{\alpha}{\varepsilon} + q_{ss}^{2-\theta}} = 1 - e^{-\frac{1}{q_{ss}}} \tag{A.1-c}$$

where the variables have the same meaning than in the main text and, again, sub-index ss means a condition evaluated at flow steady-state conditions.

The linear analysis of the stability of the steady state equations may be performed in similar terms as in [1]. To this end we first introduce a perturbation to steady-state flow conditions in the form:

$$\begin{aligned} q &= q_{ss} + q' \\ T &= T_{ss} + T' \end{aligned} \tag{A.2}$$

Introducing these definitions into the non-dimensional form of equations (A.1-A.2) we get:

$$\frac{dq'}{dt} = \varepsilon (2 - \theta) q_{ss}^{1-\theta} q' = \alpha \int_0^1 T' ds ; \tag{A.3}$$

$$\frac{\partial T'}{\partial t} + q_{ss} \frac{\partial T'}{\partial s} = 0 \tag{A.4}$$

and:

$$T'_0 + mT'_1 + nq = 0 \tag{A.5}$$

where:

$$\begin{aligned} m &= \frac{1 - T_{ss}}{1 + T_{ss}} \\ n &= \frac{1 - T_{ss}}{q_{ss}^2} \end{aligned} \tag{A.6}$$

and the sub-indexes 0 and 1 means temperatures evaluated at $s = 0, 1$ respectively.

In order to study the growth of perturbations, an exponential form in terms of time is adopted. Then:

$$\begin{aligned} q' &= \bar{q} \cdot e^{r \cdot t} \\ T' &= \bar{T} \cdot e^{r \cdot t} \end{aligned} \tag{A.7}$$

In the A.7, r is a complex and \bar{T} is the non-disturbed value of T .

Then:

$$r \cdot \bar{T} + q_{ss} \frac{\partial \bar{T}}{\partial s} = 0 \tag{A.8}$$

$$\bar{T}'_0 + m \cdot \bar{T}'_1 + n \cdot \bar{q} = 0 \tag{A.9}$$

and:

$$1 + m \cdot e^{-r/q_{ss}} + \frac{n \alpha q_{ss}}{r [r + \varepsilon_2 q_{ss}^{(1-\theta)}]} (1 - e^{-r/q_{ss}}) = 0 , \quad (\text{A.10})$$

where:

$$\varepsilon_2 = (2 - \theta) \varepsilon$$

The neutral stability curves may be found putting:

$$r = i \cdot \omega$$

Then, inserting this definition in (A.10), it is found:

$$1 + m \cdot e^{-i\omega/q_{ss}} + \frac{n \alpha q_{ss}}{i\omega [i\omega + \varepsilon_2 q_{ss}^{(1-\theta)}]} (1 - e^{-i\omega/q_{ss}}) = 0 \quad (\text{A.11})$$

Let us introduce the following definitions:

$$\begin{aligned} \bar{\omega} &= \omega / q_{ss} \\ \bar{\alpha} &= n \alpha / q_{ss} \\ \bar{\varepsilon} &= \varepsilon / q_{ss} \end{aligned}$$

(A.12)

Then, equation (17) becomes:

$$\frac{e^{i\bar{\omega}} + m}{e^{i\bar{\omega}} - 1} + \frac{\bar{\alpha}}{i\bar{\omega} (i\bar{\omega} + u \bar{\varepsilon} q_{ss}^{1-\theta})} = 0 \quad (\text{A.13})$$

Where:

$$u = (2 - \theta) \frac{a}{16} \left[\frac{DKS}{v} \right]^{1-\theta} \quad (\text{A.14})$$

Imposing that the imaginary part of (A.13) must equal 0, it results:

$$(\bar{\varepsilon}^2 u^2 q_{ss}^{2(1-\theta)} + \bar{\omega}^2) \cdot (1 - m) - 2\bar{\alpha} = 0 \quad (\text{A.15})$$

Furthermore, from equation (1-b):

$$\frac{1}{q_{ss}} = - \text{Ln} \frac{1 - T_{ss}}{1 + T_{ss}} \quad (\text{A.16})$$

Then,

$$\bar{\alpha} = \frac{1 - T_{ss}}{T_{ss}} \frac{u}{2 - \theta} q_{ss}^{-\theta} \bar{\varepsilon} \quad (\text{A.17})$$

Now, equation (A.15) may be written as:

$$\bar{\varepsilon}^2 + \frac{\bar{\omega}^2}{u^2 (q_{ss})^{2(1-\theta)}} - A \bar{\varepsilon} = 0 \quad (\text{A.18})$$

where:

$$A = \frac{1 - T_{ss}^2}{T_{ss}^2} \frac{1}{(2 - \theta)} (q_{ss})^{-(2-\theta)} \quad (\text{A.19})$$

Finally, equation (A.18) is written as the equation of an ellipse, then:

$$\left[\bar{\varepsilon} - \frac{A}{2} \right]^2 + \frac{\bar{\omega}^2}{(u q_{ss})^{(1-\theta)}} = \left[\frac{A}{2} \right]^2 \quad (\text{A.20})$$

Furthermore, setting the real part of equation (A.13) equal to zero and using (A.18), it is found that:

$$\bar{\varepsilon} = -\frac{1}{T_{ss}} \cdot \frac{1}{u \cdot q_{ss}^{1-\theta}} \cdot \bar{\omega} \cdot \cot g \left(\frac{\bar{\omega}}{2} \right) \quad (\text{A.21})$$

Equations (A.20) and (A.21) are solved by iteration to find the values of $\bar{\alpha}$ and $\bar{\varepsilon}$. Fixing a value for T_{ss} , what implies a definition for q_{ss} , performs it. After these values are found, the corresponding values of α and ε , as well as the values of all other variables of interest may also be found.

RESULTS AND DISCUSSION

Results have been obtained taking a base case, as specified in Table 1. At first glance it is not essential to set a physically sound situation, because the results may be also interpreted in non-dimensional terms. However, as mentioned before, the use of the present results to set a test, benchmark problem for a large thermal-hydraulic system code, led our studies. This approach was useful, so it was decided to keep the same philosophy. The dimensions of the loop may be considered typical of a real experimental rig. Results have been obtained keeping the same geometry and changing the heat flow (as measured by HTC) at both the source and the sink. The range adopted for the variation of HTC was such that the flow changed from fully laminar to fully turbulent.

Figure A.1 shows the neutral stability curve obtained by solving equations (A.20) and (A.21) and considering turbulent flow. Figure A.2 is a stability map, obtained by solving equations (1-3) by a modal decomposition method, using 100 and perturbing the resulting ODEs according to a standard linear stability analysis technique. It may be considered a reference solution for the differential problem and the borderline separating the stable and unstable zones must be coincident with the one in Figure A.1. In Figure A.3 the results of Figure A.1 have been re-plotted and are compared with the values obtained from Figure A.2. As may be observed the values coincide fairly well. The conspicuous point in the middle of the unstable zone corresponds to the data of Table 1.

Figure A.4 shows two neutral curves: a) one for laminar flow, obtained by setting $HTC=1000$ and b) one for turbulent flow, obtained by setting $HTC=20000$ in correspondence with the parameters given in Table 1. Once again, the isolated point in the unstable zone corresponds to the system working as given by Table 1.

Figure A.5 shows, in terms of ϵ_{Wel} (The parameter in Welander's paper [1]) and q_{ss} the neutral stability curves as a function of HTC. In this figure there are three differentiated types of curves: a) one corresponding to laminar flow ($HTC=1000$), b) one corresponding to a transitional flow ($HTC=5000$) and c) those for fully turbulent flow ($HTC=10000, 20000$ and 50000). The curve corresponding to laminar flow ($HTC=1000$) is coincident with the first part of the transitional curve (5000 L-T). At Reynolds number 2300 the friction law changes, imposing a discontinuity in the neutral curve that follows the turbulent pattern. This situation can not arise in nature and is a consequence of the standard friction law transition adopted. Figure A.6 shows a more detailed plot of this situation, considering the additional case $HTC=3000$. It is important to point out that the friction crisis exists, then, intermediate values can not be defined, except by using a suitable interpolation (as RELAP5 and every predictive code do). This problem does not arise when the Reynolds number is used as the dependent variable. What is more questionable is, perhaps, using a standard steady state law of friction for this analysis. However, this is usually the standard practice.

CONCLUSIONS

The analysis of Reference [1] was extended to consider turbulent flow. This allowed analyzing the behavior of a simple system and to specify a problem used as a benchmark for a large-scale system thermal-hydraulic code. In this way, the effects of numerical damping on unstable flows were quantified. While obtaining the results shown, the influence of the laminar to turbulent flow transition became evident. Then, considering smooth flow transition criteria and the effects of time variation on the friction law may be of importance for the complete definition of the problem.

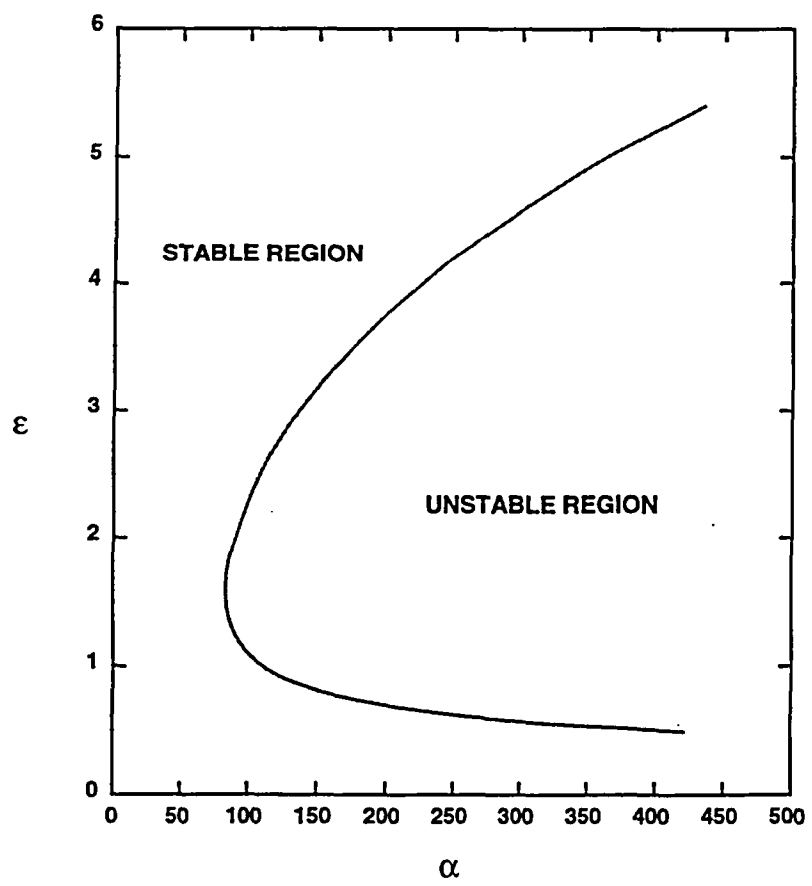


FIGURE A.1 The neutral stability curve for turbulent flow

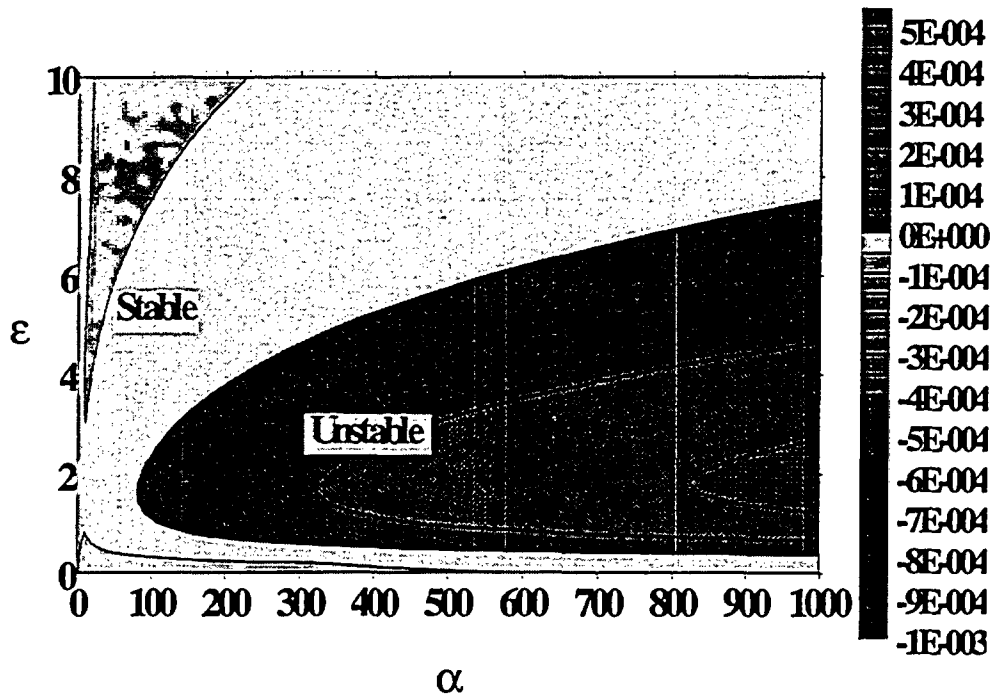


FIGURE A.2 A stability map from obtained from a reference modal solution of the flow equation, Reference [5]

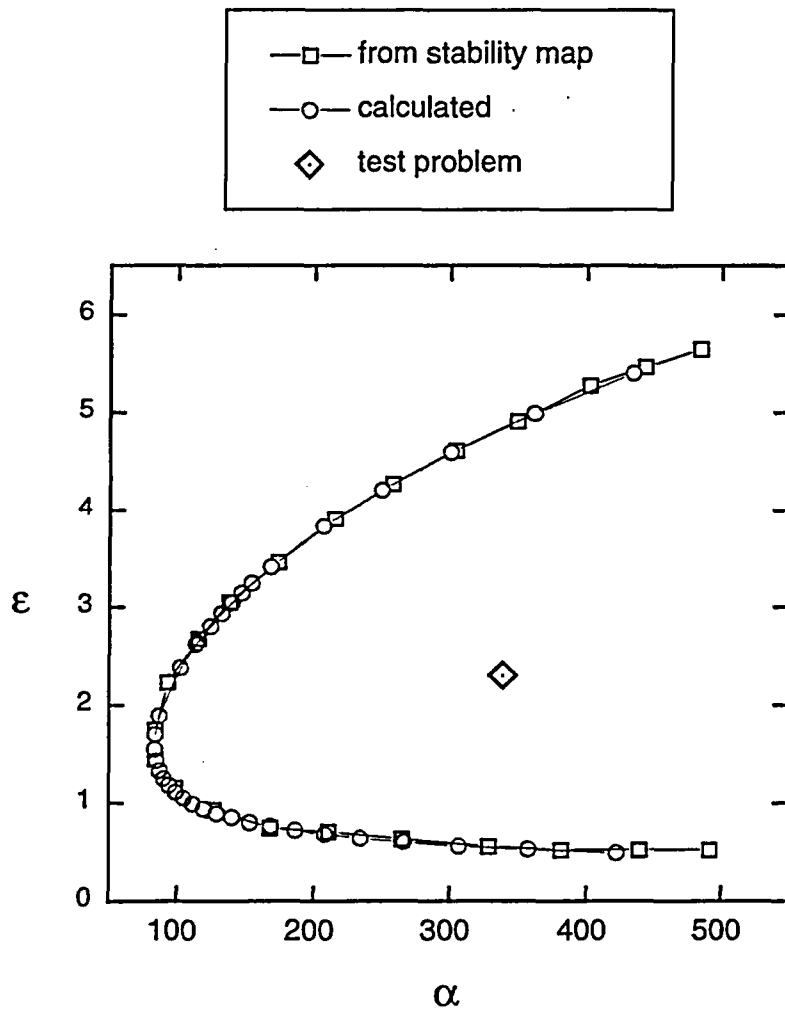


FIGURE A.3 Comparison of the theoretical and the neutral stability limit as obtained from Figure A.2

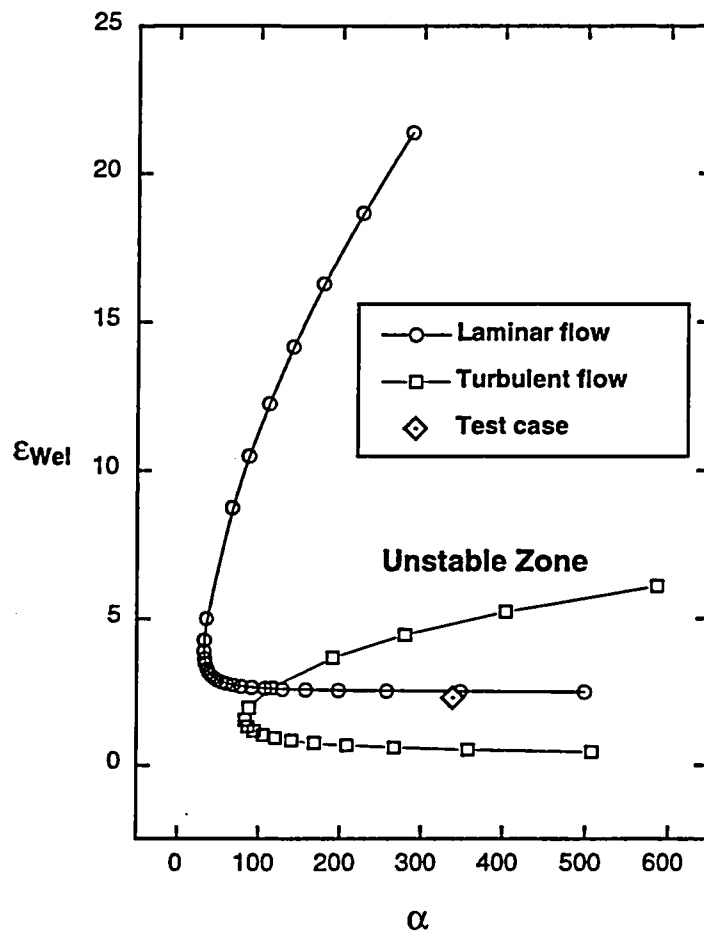


FIGURE A.4 Neutral curves for the fully laminar and fully turbulent flows

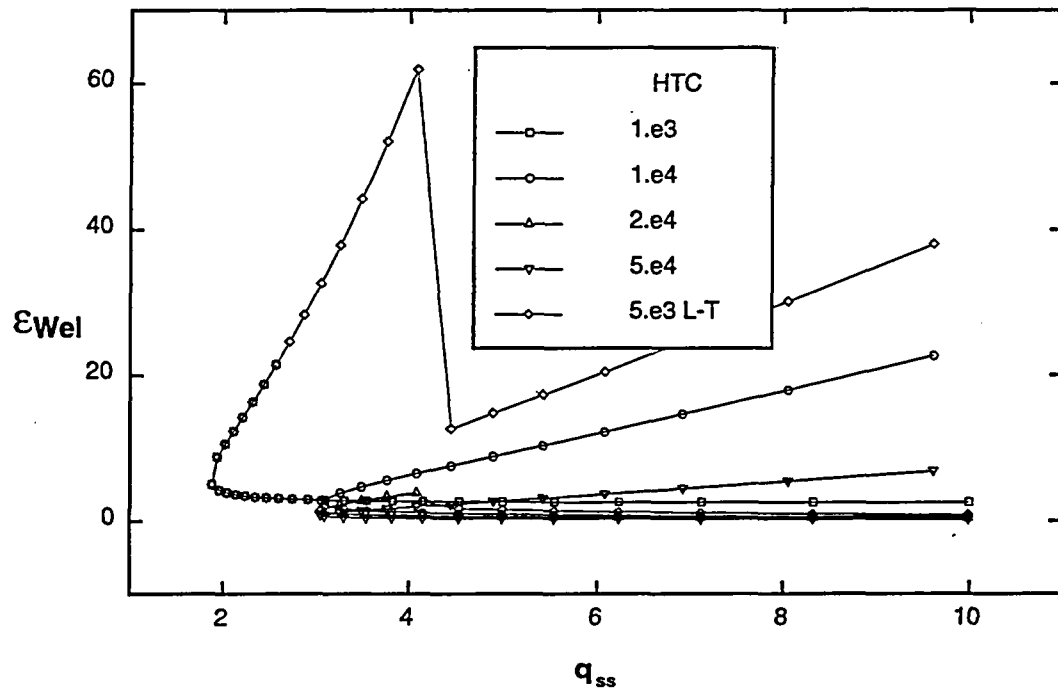


FIGURE A.5 Neutral stability curves for laminar, transitional and turbulent flows

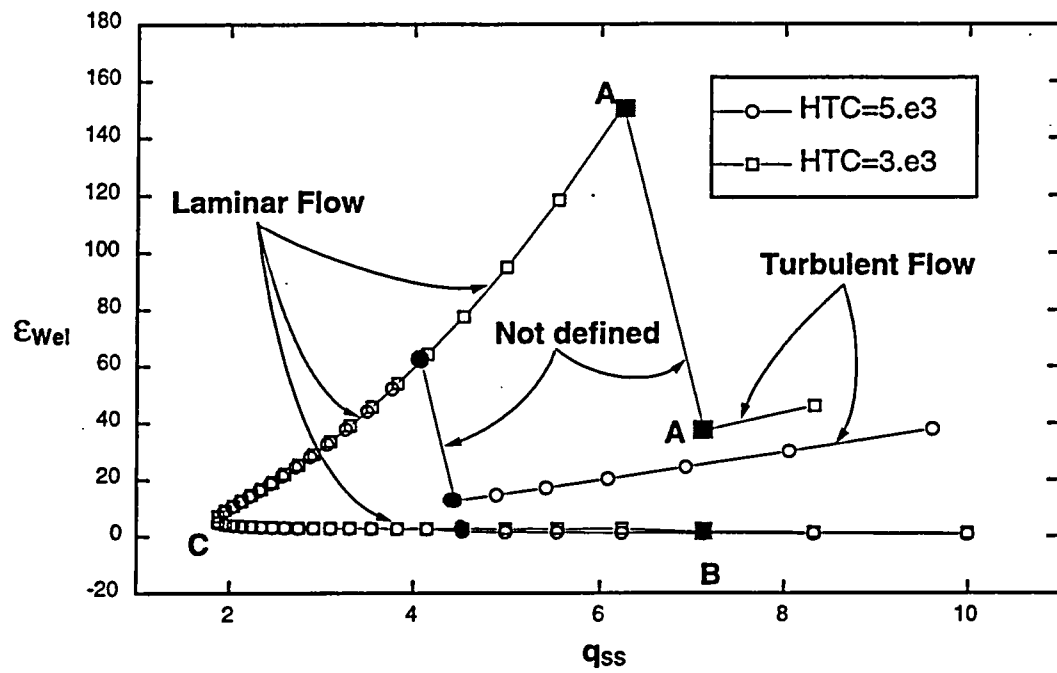


FIGURE A.6 Neutral stability curves for transitional flows

APPENDIX B

MEMORANDUM

Date: July 1991

**SUBJECT: LIMITATIONS OF THE USE OF A "HEAT EXCHANGER"
APPROXIMATION FOR A POINT HEAT SOURCE**

Produced by: G.M. Grandi and J.C. Ferreri

Sector: División Modelos Físicos y Numéricos, Ger. Seg. Rad. y Nuclear, CNEA,
Av. del Libertador 8250, 1429 Buenos Aires, Argentina

The objective of the following analysis is showing why a one cell approximation (loosely speaking a lumped parameter approximation) of a heat exchanger can not be used to get the correct value of the steady state temperature jump. This elementary condition holds for any representation using a first order upwind approximation. A correction factor is derived to deal with this situation. The working hypotheses of Welander's [1] original formulation are adopted in order to define a theoretical benchmark.

Let us consider the equation for the temperature approximation in the tubes:

$$\frac{\partial T}{\partial t} + \frac{q}{A} \frac{\partial T}{\partial s} = k \cdot (T_0(s) - T) \quad (\text{B.1})$$

where, accordingly with Welander's [1] nomenclature, q is the volumetric flow rate, T is the fluid temperature (assumed as uniform over each tube cross section), $T_0(s)$ is the temperature at the source wall, A is the tube cross section area, k is a

proportionality coefficient (assumed as constant) for the heat transfer, t is the time and s is the space co-ordinate measured along the tube length.

For steady-state (ss) it is:

$$U_{ss} \frac{\partial T}{\partial s} = k \cdot (T_0(s) - T) \quad (B.2)$$

where:

$$U_{ss} = q_{ss} / A \quad (B.3)$$

T_0 is set as $T_0 = \pm \Delta T$ in the source/sink. The rest of the tubes are adiabatic. Then, dividing the previous equation by T_0 and letting Θ it is:

$$U_{ss} \frac{\partial \Theta}{\partial s} = k \cdot (1 - \Theta) \quad (B.4)$$

Expression (4) is valid in the source.

Let us consider a cell piecewise continuous variation of T along the source, then, under an upwind approximation (Figure B.1), it is:

$$U_{ss} \left(\frac{\Theta_P - \Theta_W}{\Delta x} \right) = k \cdot (1 - \Theta_P) \quad (B.5)$$

But: $\Theta_W = -\Theta_P$, then:

$$\Theta_P = \frac{1}{1 + \frac{2 \cdot U_{ss}}{k \cdot \Delta s}} = \frac{1}{1 + 2 \cdot V} \quad (B.6)$$

where V is the non-dimensional velocity.

If the approximation for the temperature in the cell is defined as the mean of Θ_P and Θ_W , then:

$$\Theta_P = \frac{1}{2 \cdot V} \quad (B.7)$$

The following table shows the values obtained with both approximations as a function of α/ε .

α/ε	V	Θ (Welander)	$\Theta_P = \frac{1}{1+2 \cdot V}$	$\Theta_P = \frac{1}{2 \cdot V}$
0.1	0.1	0.999	0.833	5.0
1.0	0.648	0.648	0.436	0.772
2.0	0.958	0.479	0.343	0.52
10.0	2.222	0.222	0.184	0.227
0.01	0.01	1.00	0.98	50.0
0.5	0.417	0.834	0.545	2.398
50.0	4.98	0.0096	0.0912	0.010

TABLE B.1: Values of θ_P computed using different approximations for the source temperature.

As may be observed from Table B.1, expression (B.7) is a better approximation for higher flow-rates. The inverse happens with expression (B.6).

Now, let's pose the following question:

Which is the expression to be used for the heat generated at the source, under a FTUS approximation, to recover the exact value (i.e. Welander's theoretical value) of Θ_P ?

The answer comes considering the following analysis. Referring once again to Figure B.1 and integrating (B.2), it comes:

$$\int_{T_w}^T \frac{dT}{T - T_0} = - \int_0^{\Delta s} \frac{k}{U_{ss}} ds$$

where Δs is the heated length, then:

$$T = T_0 + (T_w - T_0) \cdot \exp(-1/V)$$

where $V = U_{ss} / (k \cdot \Delta s)$.

The mean value of an equivalent heat source on Δs is:

$$\langle k \cdot (T - T_0) \rangle = \frac{U_{ss}}{\Delta s} (T_0 - T_w) \cdot [1 - \exp(-1/V)] \quad (B.8)$$

Let us verify if this expression gives correct values for the fluid temperature (i.e. coincident with the values given by Welander's analysis) at the source, when the latter is computed via an upwind approximation. Using a FTUS discretization, the previous expression leads to:

$$T_P - T_w = (T_0 - T_w) \cdot F \quad (B.9)$$

where:

$$F = 1 - \exp(-1/V)$$

If we consider that $T_P = -T_W$ and introducing non-dimensional variables, then, replacing in (B.8):

$$\Theta_P = \frac{F}{2-F}$$

This expression gives values coincident with the ones of Welander's analysis.

In conclusion, using a definition for ΔT that may be obtained from (B.8) allows obtaining correct values for the steady state temperature jump at the source. This applies to a discrete upwind approximation. This, in turn, brings correct values for the steady state flow rate.

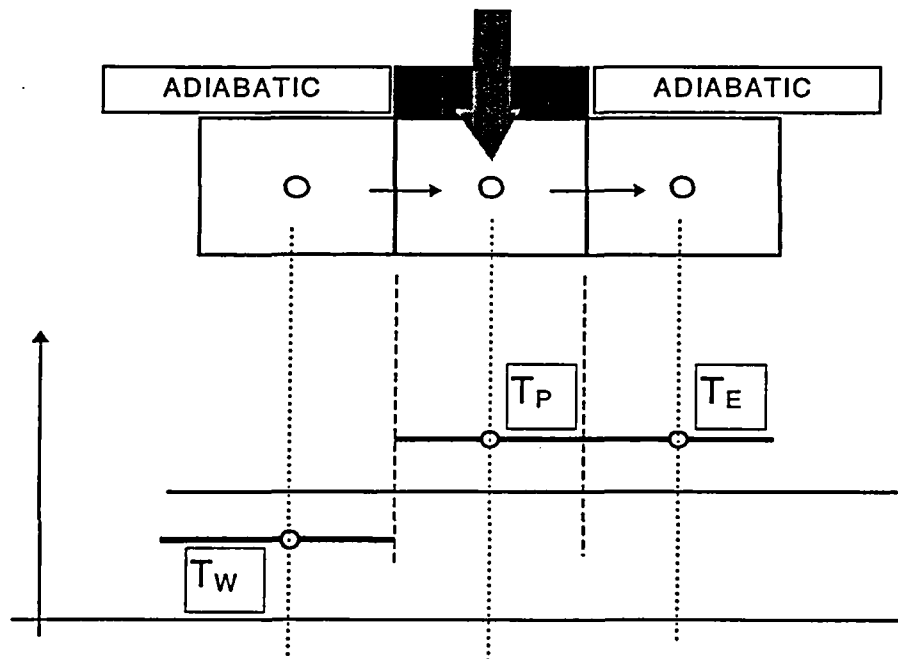


Figure 1 A sketch of the node definitions for simple upwinding

APPENDIX C

RESULTS FROM THE APPLICATION OF RELAP5/MOD3.x CODE

- LIST OF CASES CONSIDERED AND THEIR NODALIZATIONS
- PLOTS OF SELECTED RESULTS

The following nomenclature applies to the curves shown
in Figures C.1 to C.10

Fluid Pressure

100010000	* lower plenum
130010000	* upper plenum

Fluid Temperatures

100010000	* lower plenum or source
110010000	* ascending leg 1
110050000	* ascending leg 5
110100000	* ascending leg 10
130010000	* upper plenum or sink
120100000	* descending leg 10
120050000	* descending leg 5
120010000	* descending leg 1

Mass Flow Rates

100010000	* lower plenum to ascending leg
100020000	* lower plenum to descending leg
300000000	* upper plenum to TDV

Test No. 1 (code RELAP5/MOD3.0)

Cross section of components 100, 110, 120, 130 = $7.854 \times 10^{-3} \text{ m}^2$

Hydraulic diameter of components 100, 110, 120, 130 = 0.1 m

Length of components 100 and 130 = 1 m

No. of nodes in the legs (110 and 120) = 10

Roughness parameter = 10^{-7} m

Pressure in components 400 = 10^5 Pa

Initial fluid temperature 293.15 K

Geometry of heat structures : cylindrical

Heat transfer area = 0.628 m^2 (internal diameter = 0.2 m, length = 1 m)

Thickness = 10^{-4} m

Thermal conductivity = $100 \text{ W}/(\text{m}^2\text{K})$

Volumetric heat capacity = $10^5 \text{ J}/(\text{m}^3\text{K})$

Initial lower and upper structure temperature = 293.15 K

Final upper structure surface temperature = 293.15 K

Final lower structure outer surface temperature = 303.15 K (after 0.1 s)

Imposed heat transfer coefficient at lower and upper structures = $1000 \text{ W}/(\text{m}^2\text{K})$

Time step = 0.5 s

Initial loop flow rate = 0.1 kg/s

Test No. 2 (code RELAP5/MOD3.0)

As Test No. 1 with:

Length of components 100 and 130 = 0.5 m

Structure heat transfer area = 0.314 m^2 (internal diameter = 0.2 m, length = 0.5 m)

Imposed heat transfer coefficient at lower and upper structures = $2000 \text{ W}/(\text{m}^2\text{K})$

Test No. 3 (code RELAP5/MOD3.0)

As Test No. 1 with:

Length of components 100 and 130 = 0.1 m

Structure heat transfer area = 0.0628 m² (internal diameter = 0.2 m,
length = 0.1 m)

Imposed heat transfer coefficient at lower and upper structures = 10000 W/(m²K)

Test No. 4 (code RELAP5/MOD3.0)

As Test No. 3 with:

No. of nodes in the legs (110 and 120) = 25

Test No. 5 (code RELAP5/MOD3.0)

As Test No. 3 with:

No. of nodes in the legs (110 and 120) = 50

Test No. 6 (code RELAP5/MOD3.0)

As Test No. 3 with:

No. of nodes in the legs (110 and 120) = 90

Test No. 7 (code RELAP5/MOD3.0)

As Test No. 6 with:

Initial loop flow rate = 0.001 kg/s

Test No. 8 (code RELAP5/MOD3.0)

As Test No. 7 with:

No. of nodes in the legs (110 and 120) = 40 (searching for neutral stability)

Test No. 9 (code RELAP5/MOD3.0)

As Test No. 7 with:

No. of nodes in the legs (110 and 120) = 38 (searching for neutral stability)

Test No. 10 (code RELAP5/MOD3.0)

As Test No. 7 with:

No. of nodes in the legs (110 and 120) = 36 (searching for neutral stability)

Test No. 11 (code RELAP5/MOD3.0)

As Test No. 7 with:

No. of nodes in the legs (110 and 120) = 34 (searching for neutral stability)

Test No. 12 (code RELAP5/MOD3.1)

As Test No. 8

Test No. 13 (code RELAP5/MOD3.1)

As Test No. 6

Test No. 14 (code RELAP5/MOD3.0)

As Test No. 7 with:

No. of nodes in the legs (110 and 120) = 37 (searching for neutral stability)

Test No. 15 (code RELAP5/MOD3.0)

As Test No. 14 with:

Time step = 1.0 s

Test No. 16 (code RELAP5/MOD3.0)

As Test No. 14 with:

Time step = 0.25 s

Test No. 19 (code RELAP5/MOD3.0)

As Test No. 9 with:

Pressure control junction 300 closed after 3000 s

ADDITIONAL CASE SERIES

Test No. X1 (code RELAP5/MOD3.0)

As Test No. 1 with:

Structure heat transfer area = 0.0314 m^2 (internal diameter = 0.1 m,
length = 0.1 m)

Test No. X2 (code RELAP5/MOD3.0)

As Test No. 2 with:

Structure heat transfer area = 0.0314 m^2 (internal diameter = 0.1 m,
length = 0.1 m)

Test No. X6 (code RELAP5/MOD3.0)

As Test No. 6 with:

Structure heat transfer area = 0.0314 m^2 (internal diameter = 0.1 m,
length = 0.1 m)

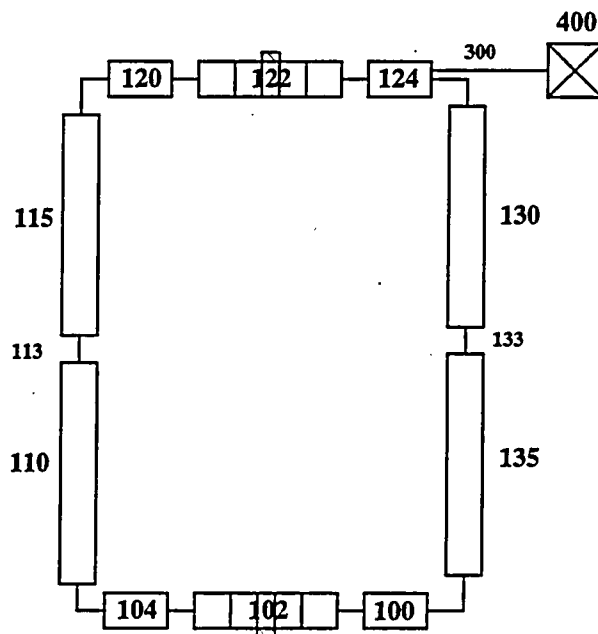
Test No. X14 (code RELAP5/MOD3.0)

As Test No. 14 with:

Structure heat transfer area = 0.0314 m^2 (internal diameter = 0.1 m,
length = 0.1 m)

Tests performed using RELAP5/MOD2 for the Benchmark Calculation

Nodalization



Test No. F2

Cross section of loop components = $1.26 \times 10^{-3} \text{ m}^2$
 Hydraulic diameter of loop components = 0.04 m
 Overall length of components 100-102-104 and 120-122-124 = 0.5 m
 Length of components 100, 104, 120, 124 = 0.1 m
 Length of nodes in pipes 102 and 122 = 0.08 m, 0.05 m, 0.04 m, 0.05 m, 0.08 m
 Length of pipes 110, 115, 130, 135 = 5 m
 No. of nodes in components 110, 115, 130, 135 = 50
 Roughness parameter = 10^{-7} m
 Pressure in component 400 = 10^5 Pa
 Initial fluid temperature 293.15 K

Geometry of heat structures: cylindrical
 Length of structures = 0.04 m
 Thickness = $5 \times 10^{-5} \text{ m}$
 Thermal conductivity = $100 \text{ W}/(\text{m}^2 \text{ K})$
 Volumetric heat capacity = $10^5 \text{ J}/(\text{m}^3 \text{ K})$

Initial lower and upper structure temperature = 293.15 K
Final upper structure surface temperature = 293.15 K
Final lower structure outer surface temperature = 303.15 K (after 100 s)
Imposed heat transfer coefficient at lower and upper structures = 2500 W/(m²K)

Time step = 0.5 s
Initial loop flow rate = 0.1 kg/s
Steady-State Period = 10 s

Test No. F3

Cross section of loop components = $3.1416 \times 10^{-4} \text{ m}^2$
Hydraulic diameter of loop components = 0.02 m
Overall length of components 100-102-104 and 120-122-124 = 0.5 m
Length of components 100, 104, 120, 124 = 0.1 m
Length of nodes in pipes 102 and 122 = 0.08 m, 0.05 m, 0.04 m, 0.05 m, 0.08 m
Length of pipes 110, 115, 130, 135 = 5 m
No. of nodes in components 110, 115, 130, 135 = 50
Roughness parameter = 10^{-7} m
Pressure in component 400 = 10^5 Pa
Initial fluid temperature 293.15 K

Geometry of heat structures : cylindrical
Length of structures = 0.02 m
Thickness = $5 \times 10^{-5} \text{ m}$
Thermal conductivity = $100 \text{ W}/(\text{m}^2\text{K})$
Volumetric heat capacity = $10^5 \text{ J}/(\text{m}^3\text{K})$

Initial lower and upper structure temperature = 293.15 K
Final upper structure surface temperature = 293.15 K
Final lower structure outer surface temperature = 303.15 K (after 100 s)
Imposed heat transfer coefficient at lower and upper structures = 2500 W/(m²K)

Time step = 0.5 s
Initial loop flow rate = 0.2 kg/s
Steady-State Period = 10 s

Test No. F4

Cross section of loop components = $3.1416 \times 10^{-4} \text{ m}^2$
Hydraulic diameter of loop components = 0.02 m
Overall length of components 100-102-104 and 120-122-124 = 0.5 m
Length of components 100, 104, 120, 124 = 0.1 m
Length of nodes in pipes 102 and 122 = 0.08 m, 0.05 m, 0.04 m, 0.05 m, 0.08 m
Length of pipes 110, 115, 130, 135 = 5 m
No. of nodes in components 110, 115, 130, 135 = 50

Roughness parameter = 10^{-7} m
Pressure in component 400 = 10^5 Pa
Initial fluid temperature 293.15 K

Geometry of heat structures : cylindrical
Length of structures = 0.04 m
Thickness = 5×10^{-5} m
Thermal conductivity = $100 \text{ W}/(\text{m}^2 \text{ K})$ ₃
Volumetric heat capacity = $10^5 \text{ J}/(\text{m}^3 \text{ K})$

Initial lower and upper structure temperature = 293.15 K
Final upper structure surface temperature = 293.15 K
Final lower structure outer surface temperature = 303.15 K (after 100 s)
Imposed heat transfer coefficient at lower and upper structures = $2500 \text{ W}/(\text{m}^2 \text{ K})$

Time step = 0.5 s
Initial loop flow rate = 0.5 kg/s
Steady-State Period = 10 s

Test No. F5

As Test No. F2 with:

Only 10 nodes in the legs (in place of 100 nodes as in test F2)

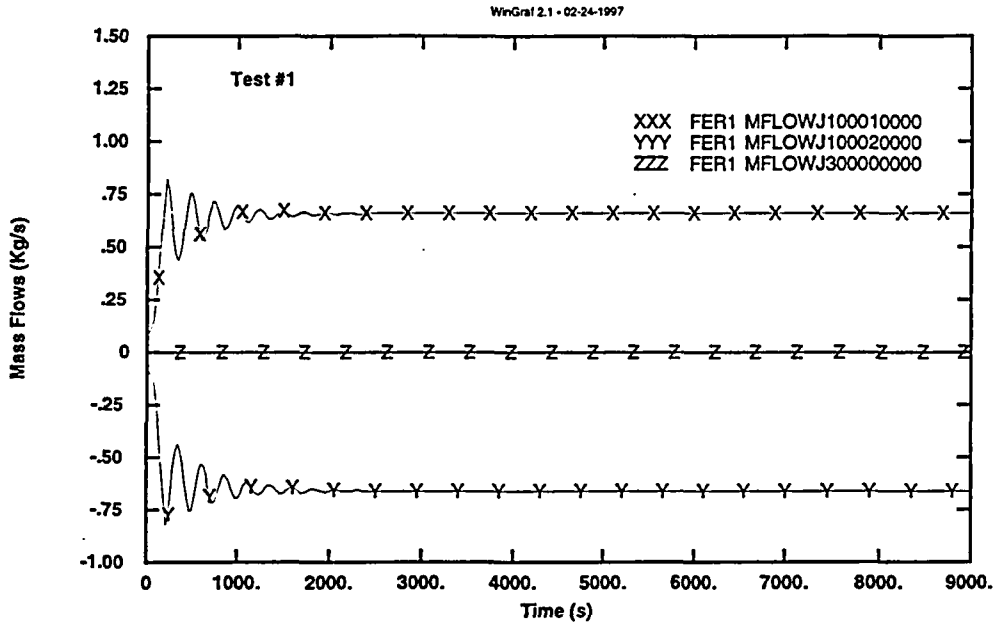


Figure C.1a TEST #1 Base Case using RELAP5/MOD3.0
 Mass Flow Rates in Legs and TDV junction, 10 nodes per leg,
 (Length of Components = 1m, Heated Length = 1m,
 Initial Mass Flow Rate=0.1Kg/s)

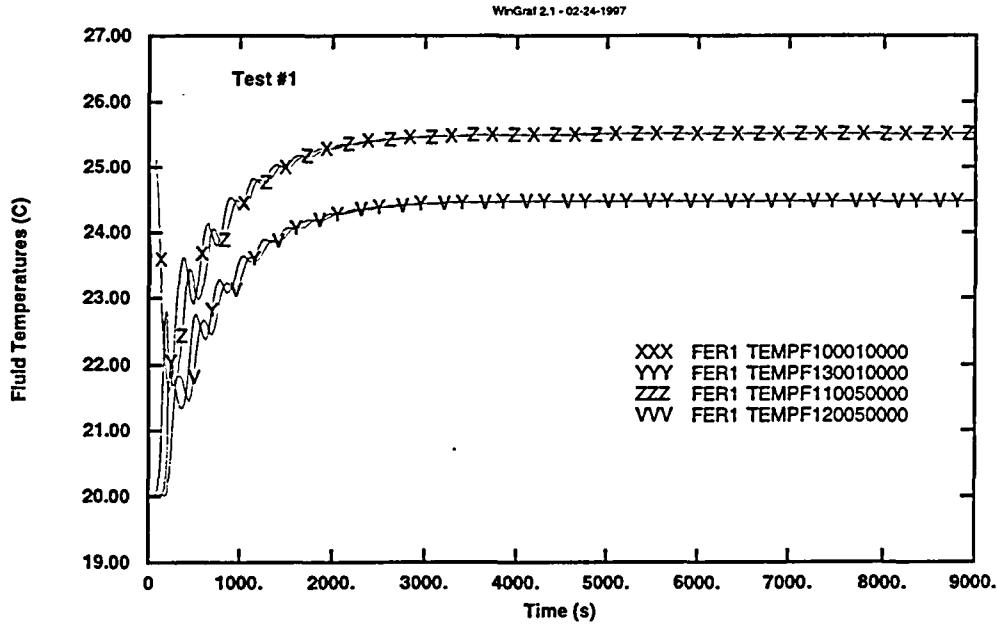


Figure C.1b TEST #1 Base Case
 Fluid Temperatures at Source, Ascending Leg Cell 5,
 Sink and Descending Leg Cell 5, conditions as in Figure C.1a.

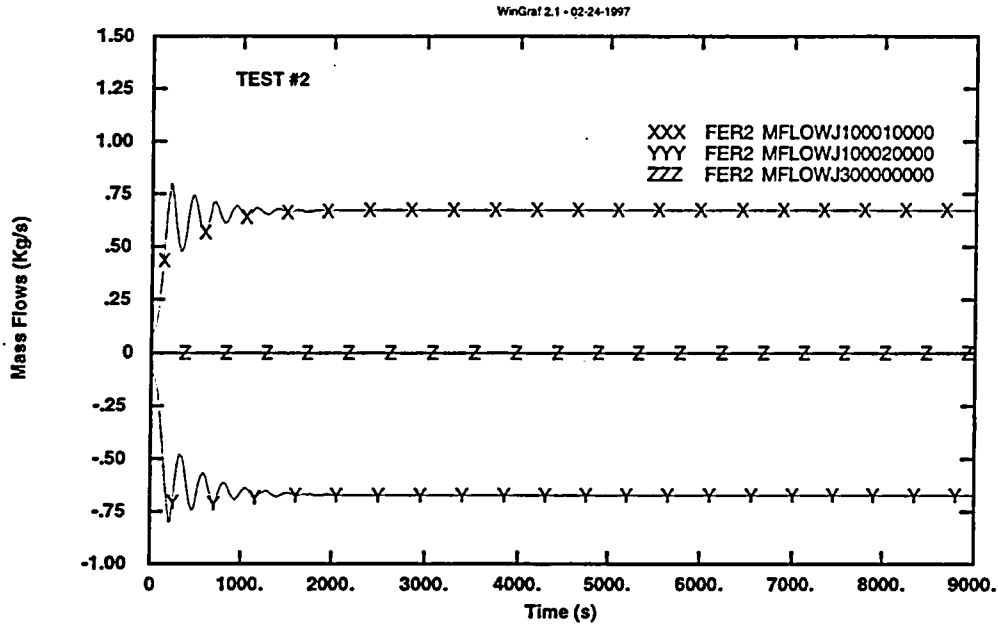


Figure C.2a TEST #2 Sensitivity of results to heated length and RELAP5/MOD3.0 Mass Flow Rates in Legs and TDV junction, 10 nodes per leg, (Length of Components = 1m, Heated Length = 0.5m, Initial Mass Flow Rate=0.1Kg/s)

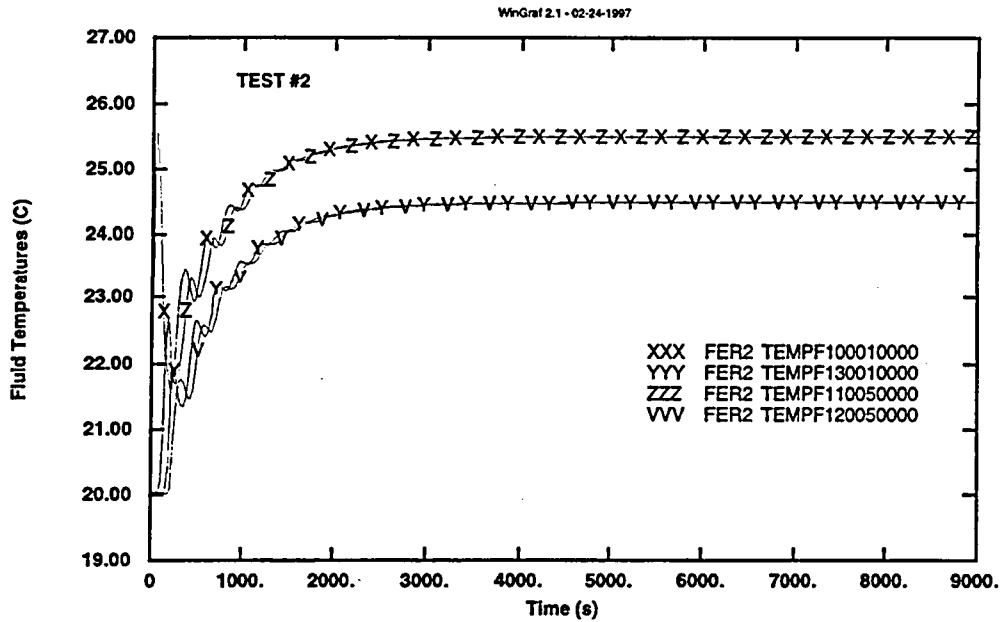


Figure C.2b TEST #2 Sensitivity of results to heated length Fluid Temperatures at Source, Ascending Leg Cell 5, Sink and Descending Leg Cell 5, conditions as in Figure C.2a.

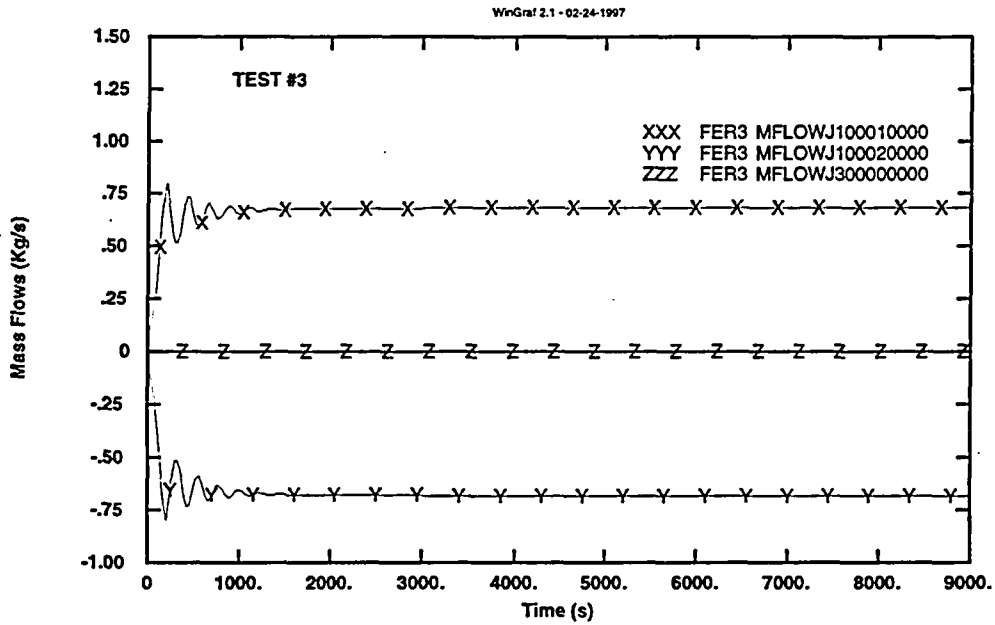


Figure C.3a TEST #3 Sensitivity of results to heated length and RELAP5/MOD3.0 Mass Flow Rates in Legs and TDV junction, 10 nodes per leg, (Length of Components = 1m, Heated Length = 0.1m, Initial Mass Flow Rate=0.1Kg/s)

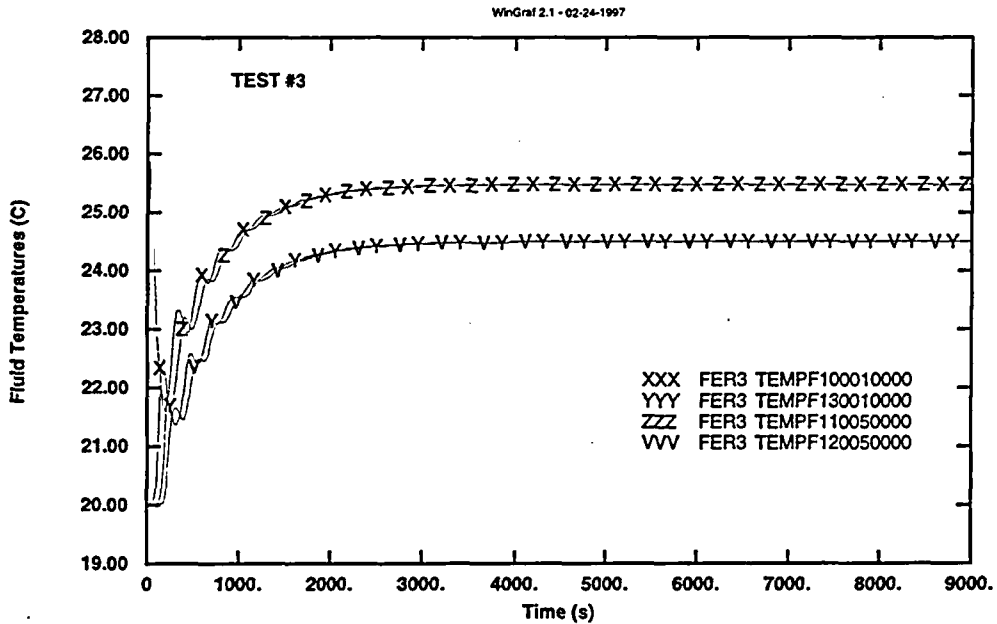


Figure C.3b TEST #3 Sensitivity of results to heated length Fluid Temperatures at Source, Ascending Leg Cell 5, Sink and Descending Leg Cell 5, conditions as in Figure C.3a.

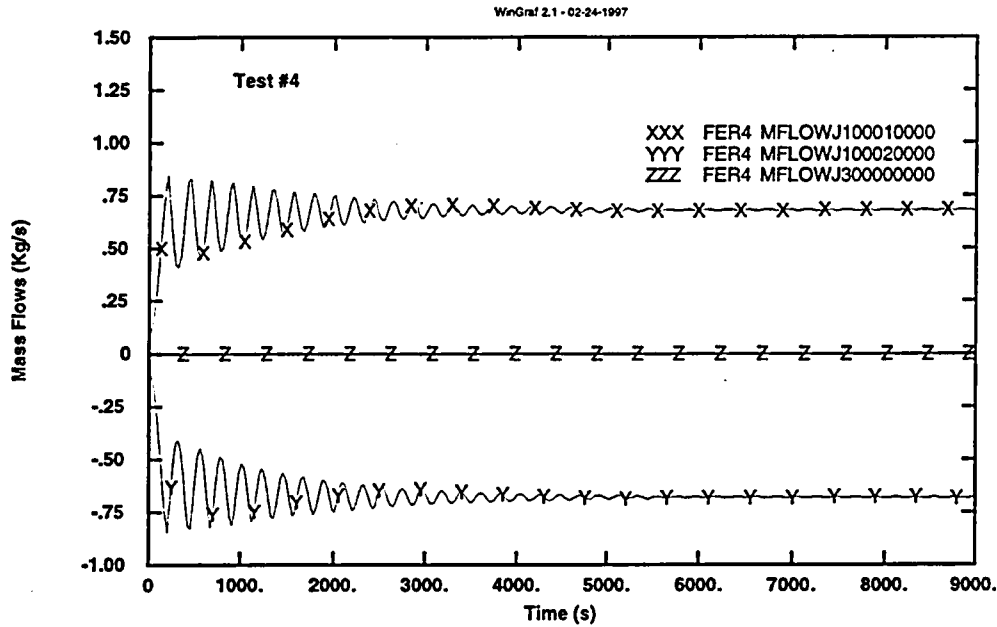


Figure C.4a TEST #4 Sensitivity of results to nodes number and RELAP5/MOD3.0 Mass Flow Rates in Legs and TDV junction, 25 nodes per leg, (Length of Components = 0.4m, Heated Length = 0.1m, Initial Mass Flow Rate=0.1Kg/s)

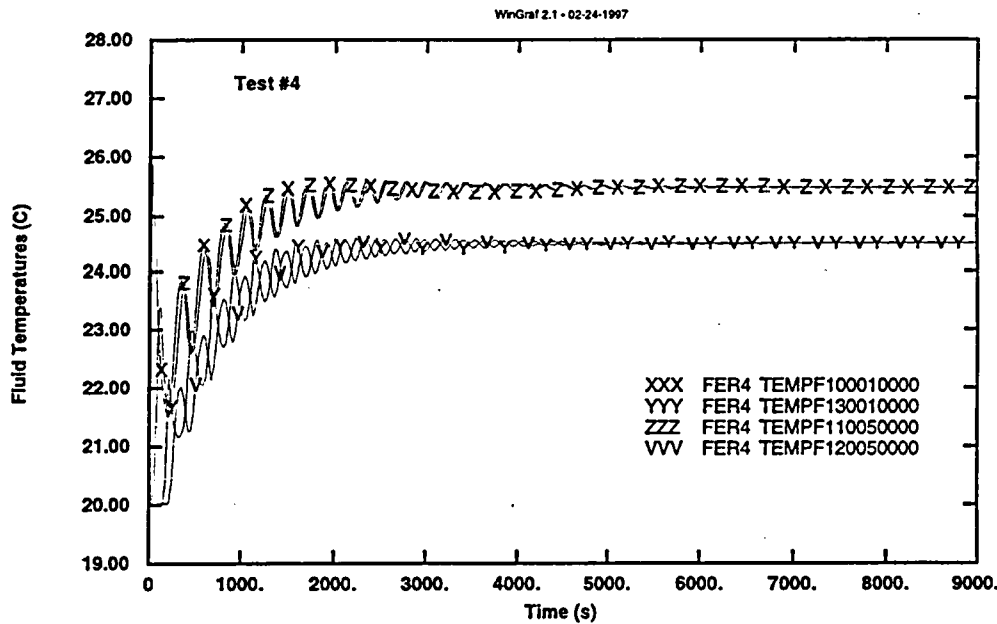


Figure C.4b TEST #4 Sensitivity of results to nodes number Fluid Temperatures at Source, Ascending Leg Cell 5, Sink and Descending Leg Cell 5, conditions as in Figure C.4a.

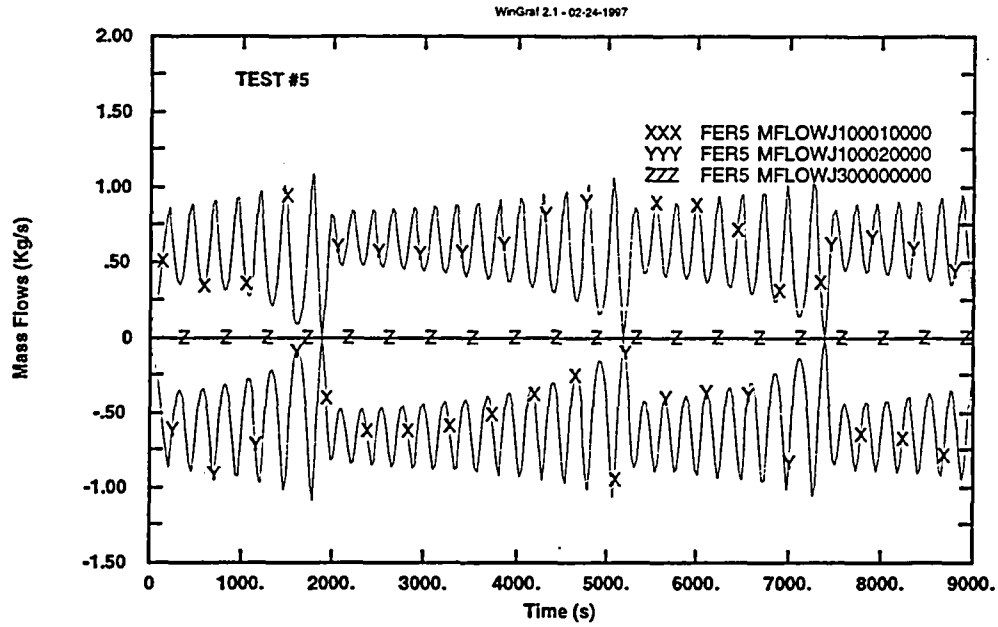


Figure C.5a TEST #5 Sensitivity of results to nodes number and RELAP5/MOD3.0 Mass Flow Rates in Legs and TDV junction, 50 nodes per leg, (Length of Components = 0.2m, Heated Length = 0.1m, Initial Mass Flow Rate=0.1Kg/s)

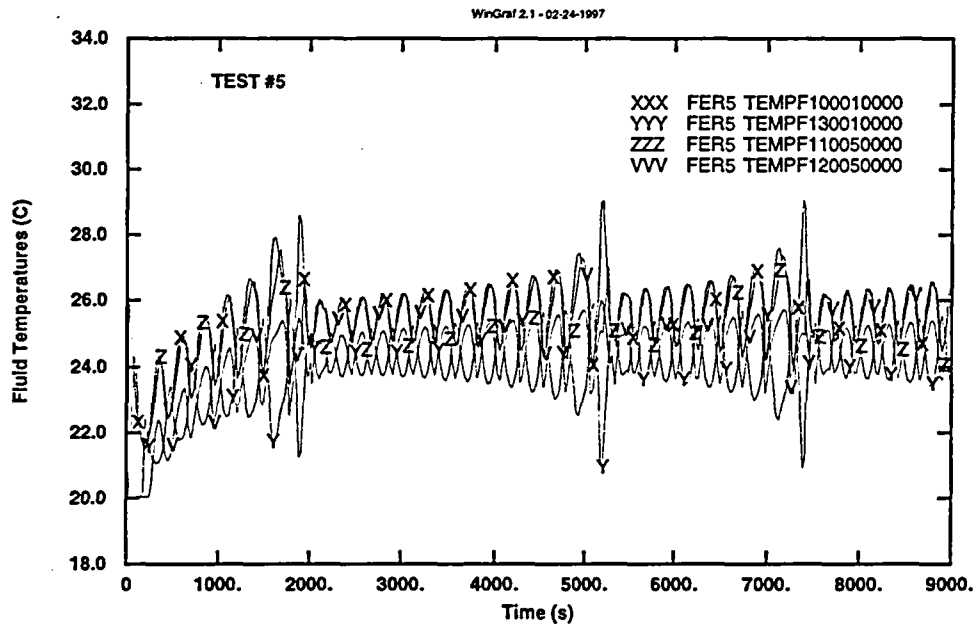


Figure C.5b TEST #5 Sensitivity of results to nodes number Fluid Temperatures at Source, Ascending Leg Cell 5, Sink and Descending Leg Cell 5, conditions as in Figure C.5a.

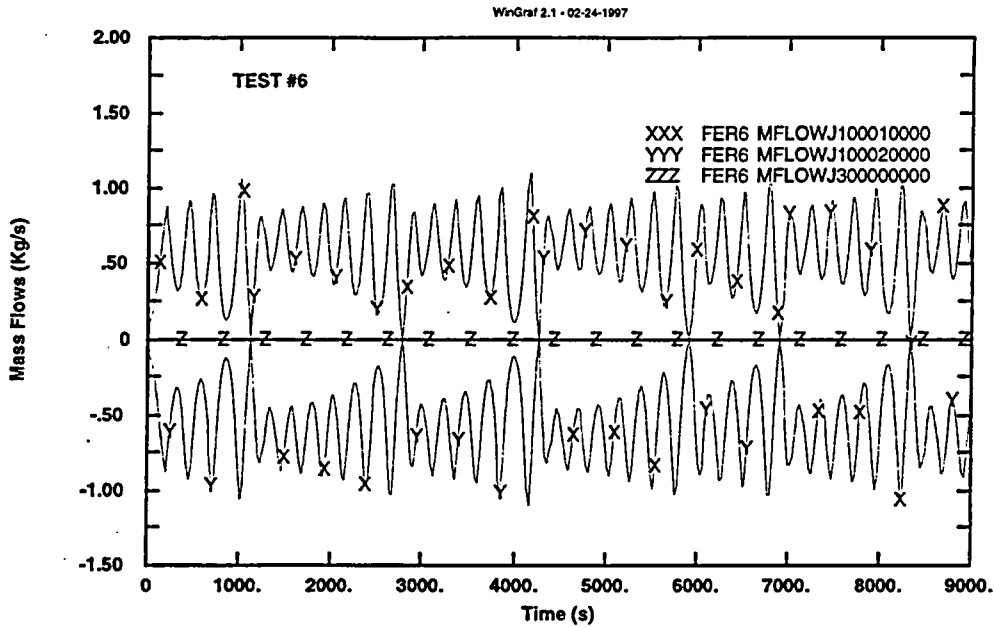


Figure C.6a TEST #6 The recovery of unstable behavior and RELAP5/MOD3.0 Mass Flow Rates in Legs and TDV junction, 90 nodes per leg, (Length of Components = 0.11m, Heated Length = 0.1m, Initial Mass Flow Rate = 0.1Kg/s)

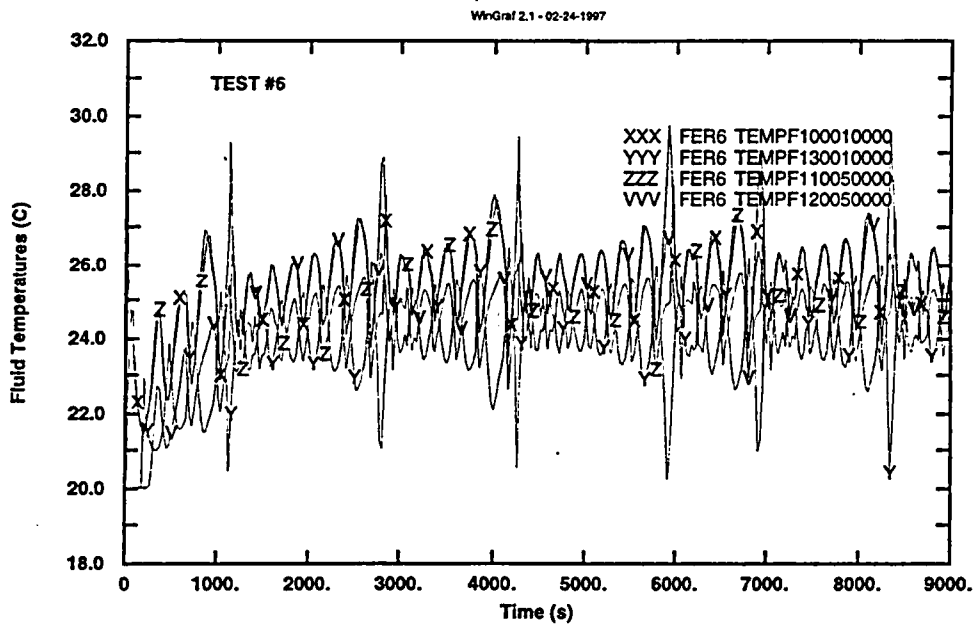


Figure C.6b TEST #6 The recovery of unstable behavior Fluid Temperatures at Source, Ascending Leg Cell 5, Sink and Descending Leg Cell 5, conditions as in Figure C.6a.

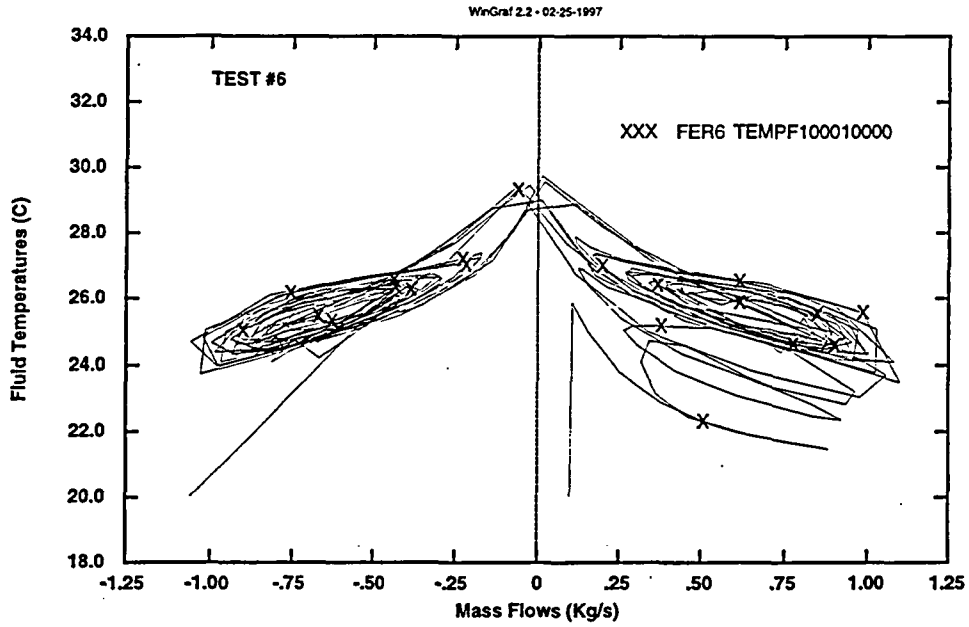


Figure C.6c TEST #6 The recovery of unstable behavior
Source Fluid Temperature vs. Mass Flow Rate,
Conditions as in Figure C.6a.

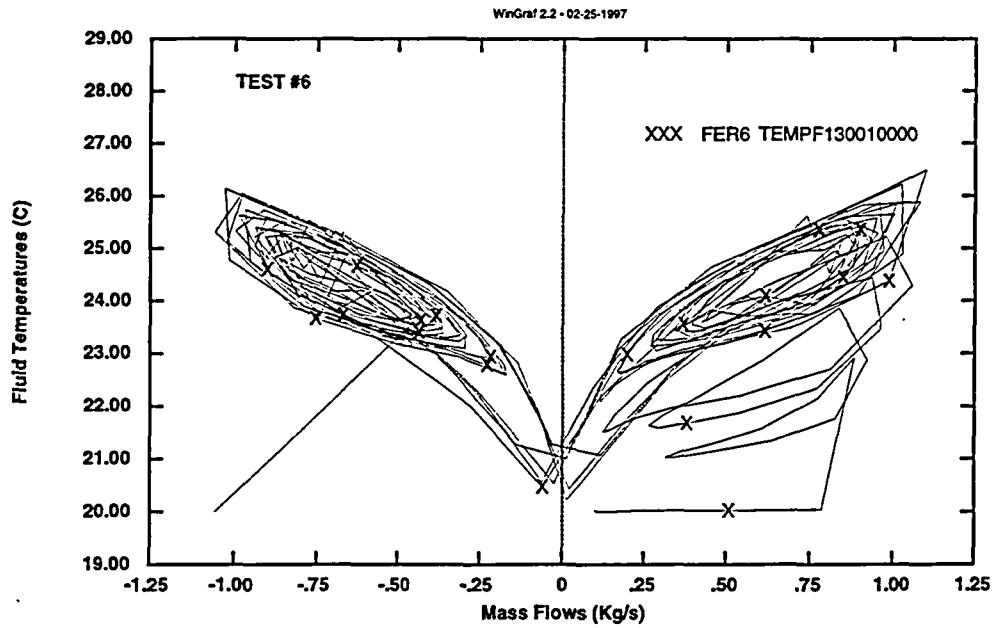


Figure C.6d TEST #6 The recovery of unstable behavior
Sink Fluid Temperature vs. Mass Flow Rate,
Conditions as in Figure C.6a.

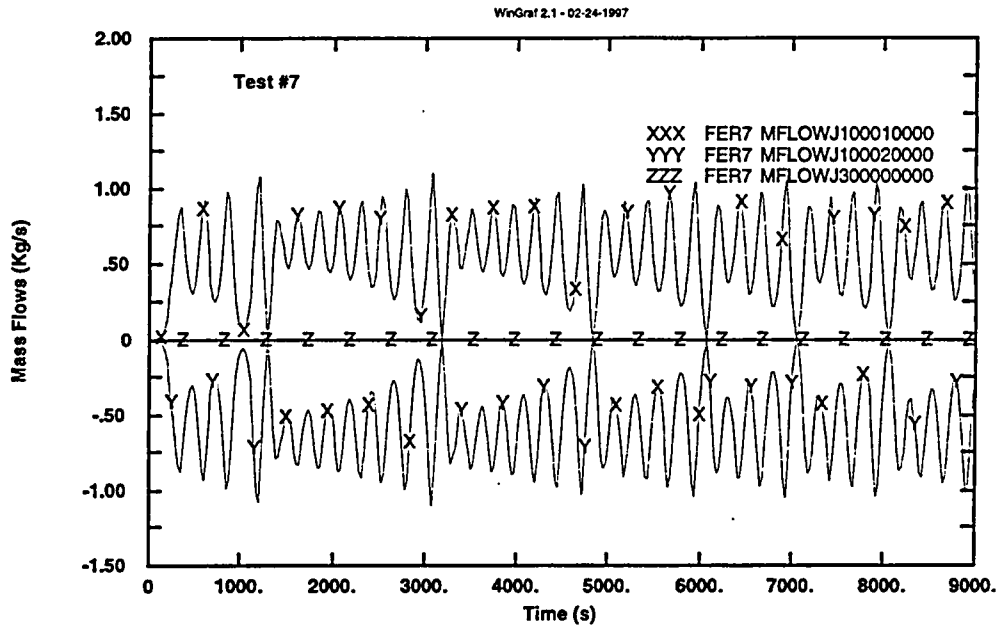


Figure C.7a TEST #7 The recovery of unstable behavior starting from (almost) rest and RELAP5/MOD3.0
 Mass Flow Rates in Legs and TDV junction, 90 nodes per leg,
 (Length of Components = 0.11m, Heated Length = 0.1m,
 Initial Mass Flow Rate = 0.001Kg/s)

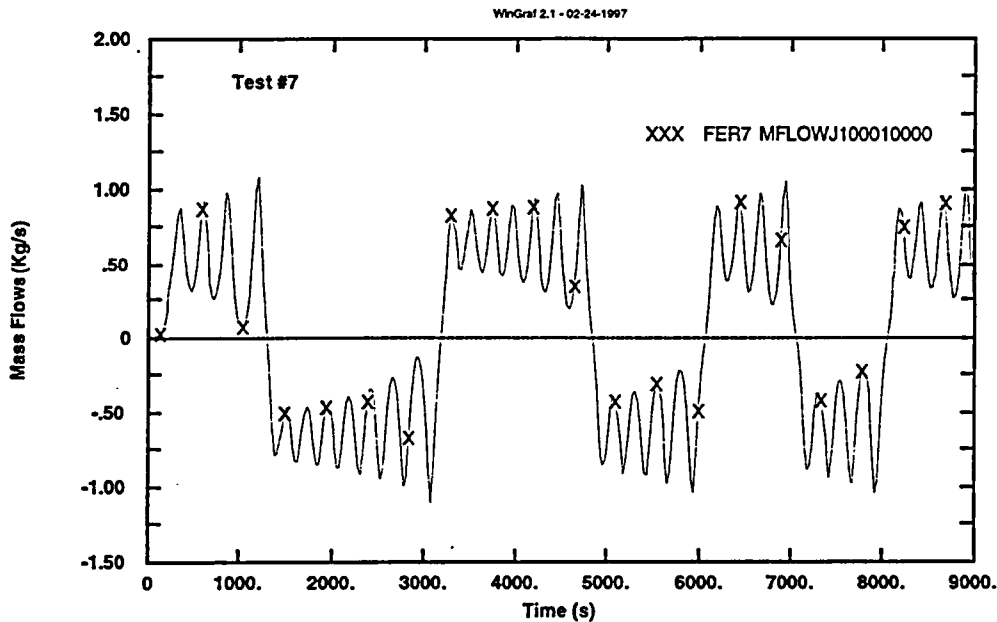


Figure C.7b TEST #7 The recovery of unstable behavior starting from (almost) rest
 Mass Flow Rate in Ascending Leg, 90 nodes per leg,
 (Length of Components = 0.11m, Heated Length = 0.1m,
 Initial Mass Flow Rate = 0.001Kg/s)

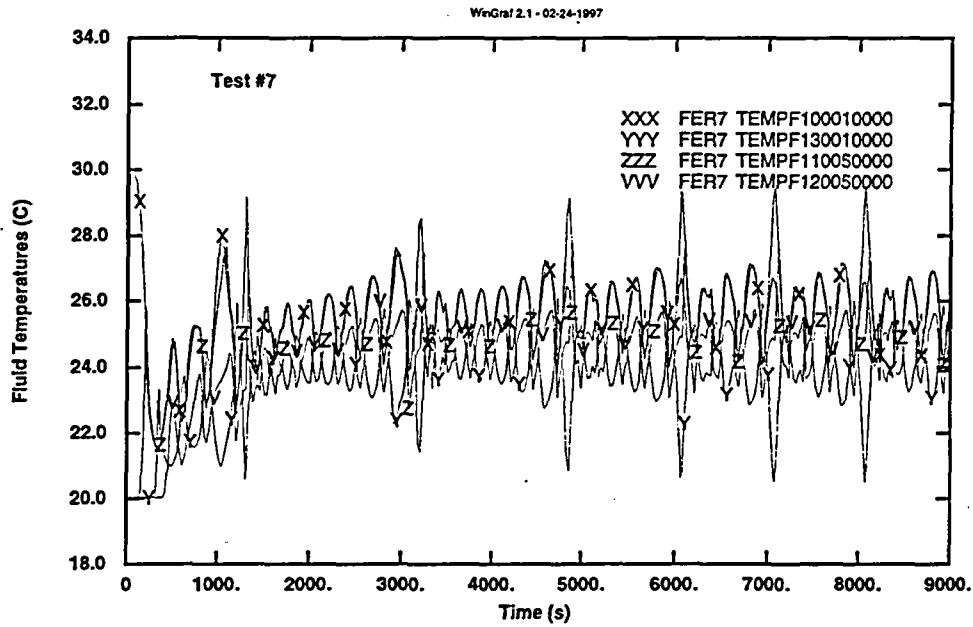


Figure C.7c TEST #7 The recovery of unstable behavior starting from (almost) rest Fluid Temperatures at Source, Ascending Leg Cell 5, Sink and Descending Leg Cell 5, conditions as in Figure C.7a.

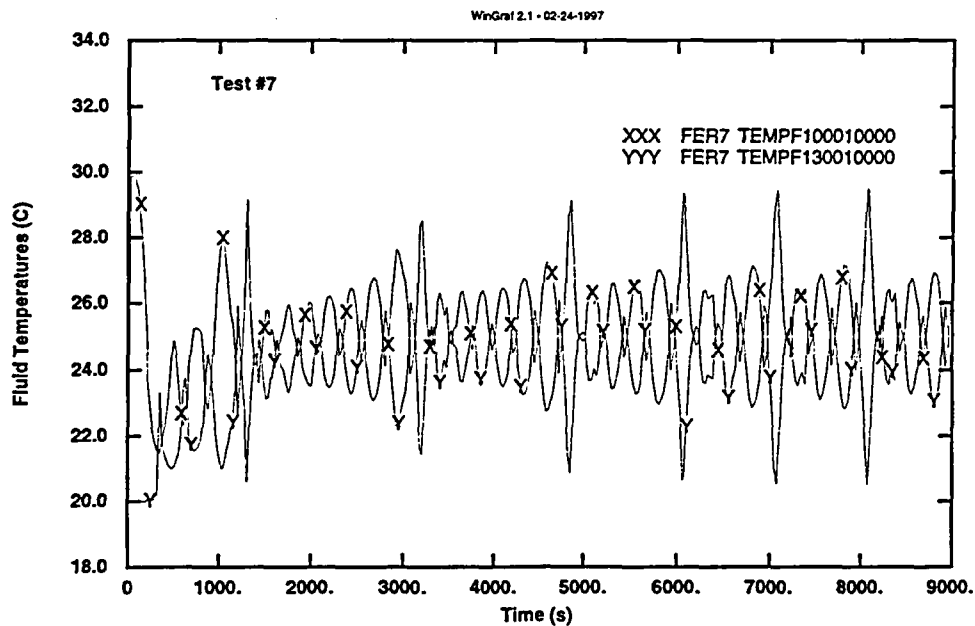


Figure C.7d TEST #7 The recovery of unstable behavior starting from (almost) rest. Fluid Temperatures at Source and Sink, conditions as in Figure C.7a.

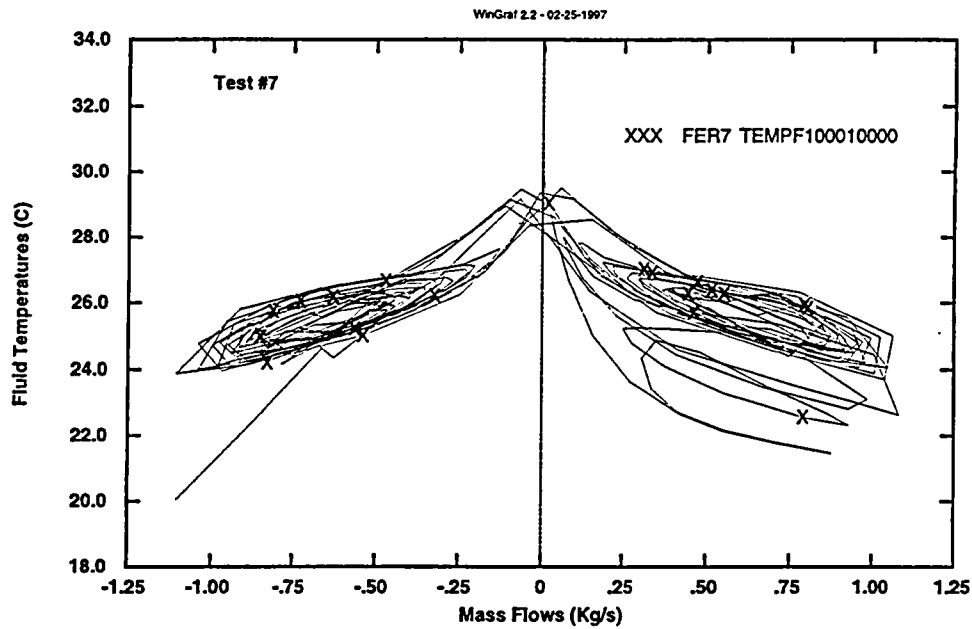


Figure C.7e TEST #7 The recovery of unstable behavior starting from (almost) rest Source Fluid Temperature vs. Mass Flow Rate, Conditions as in Figure C.7a.

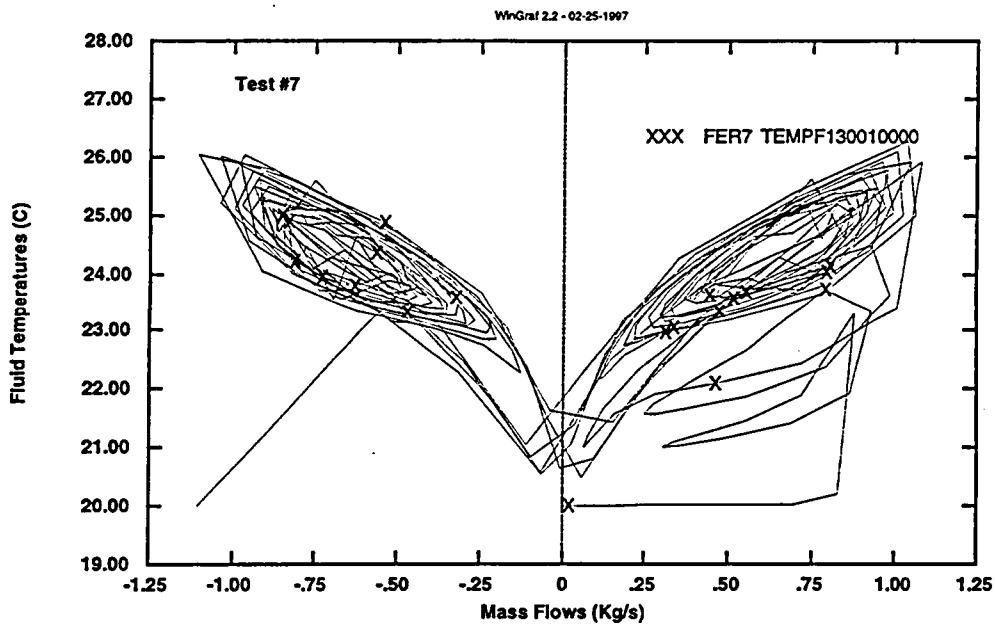


Figure C.7f TEST #7 The recovery of unstable behavior starting from (almost) rest Sink Fluid Temperature vs. Mass Flow Rate, conditions as in Figure C.7a.

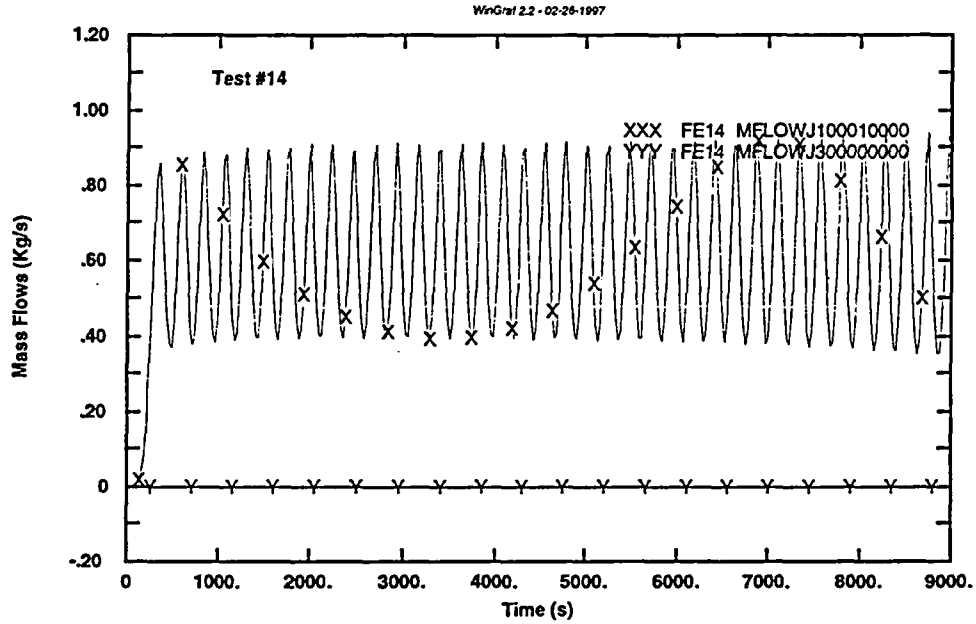


Figure C.8.a TEST #14 Search for Neutral Stability and RELAP5/MOD3.0
 Conditions as in TEST #7
 Mass Flow Rates in Ascending Leg and toward TDV, 37 nodes per leg,
 (Length of Components = 0.11m, Heated Length = 0.1m,
 Initial Mass Flow Rate = 0.001Kg/s)

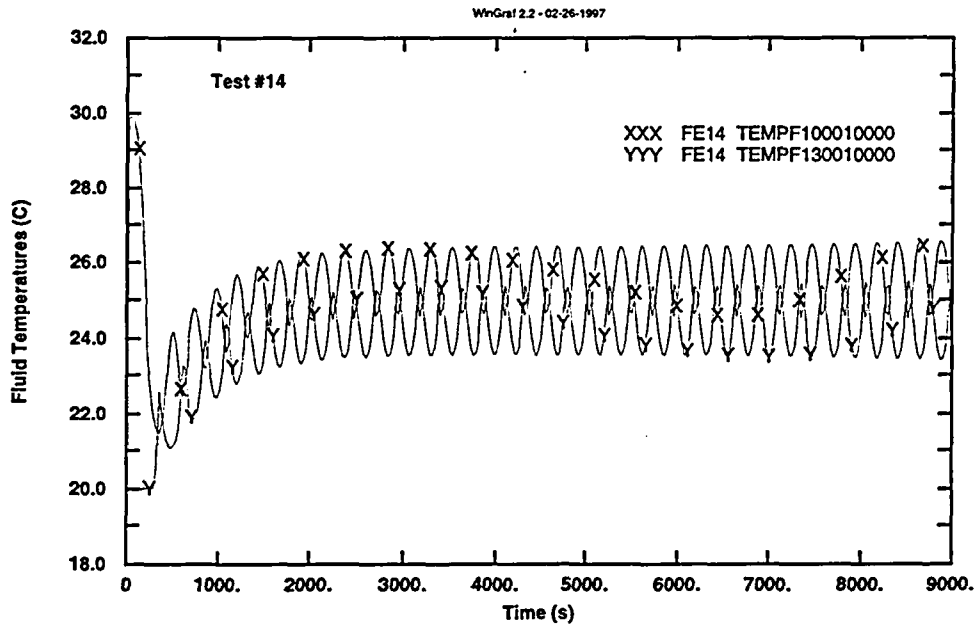


Figure C.8.b TEST #14 Search for Neutral Stability
 Fluid Temperatures at Source and Sink conditions as in Figure C.8.a.

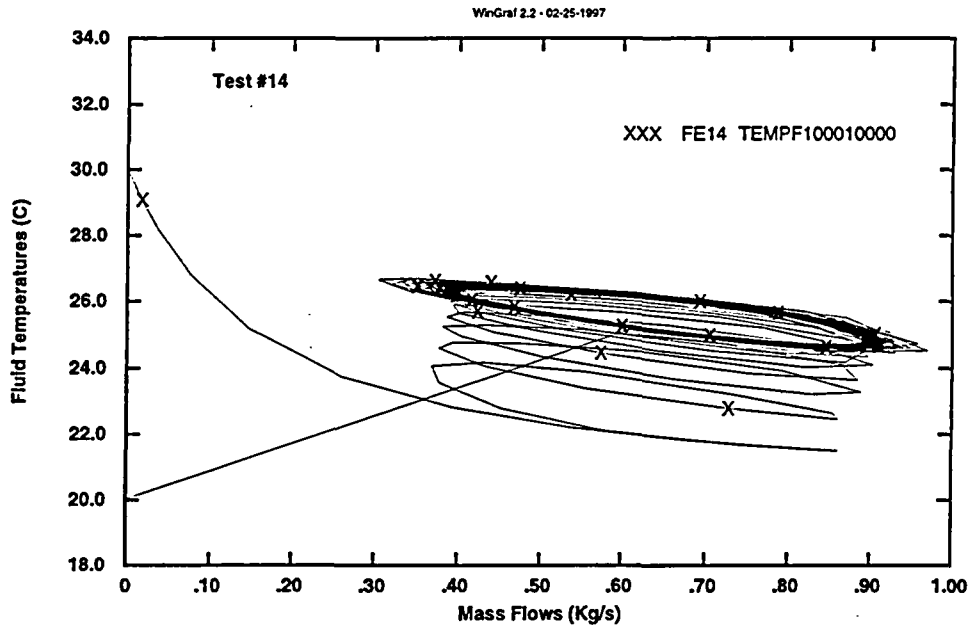


Figure C.8c TEST #14 Search for Neutral Stability
Source Fluid Temperature vs. Mass Flow Rate,
Conditions as in Figure C.8a.

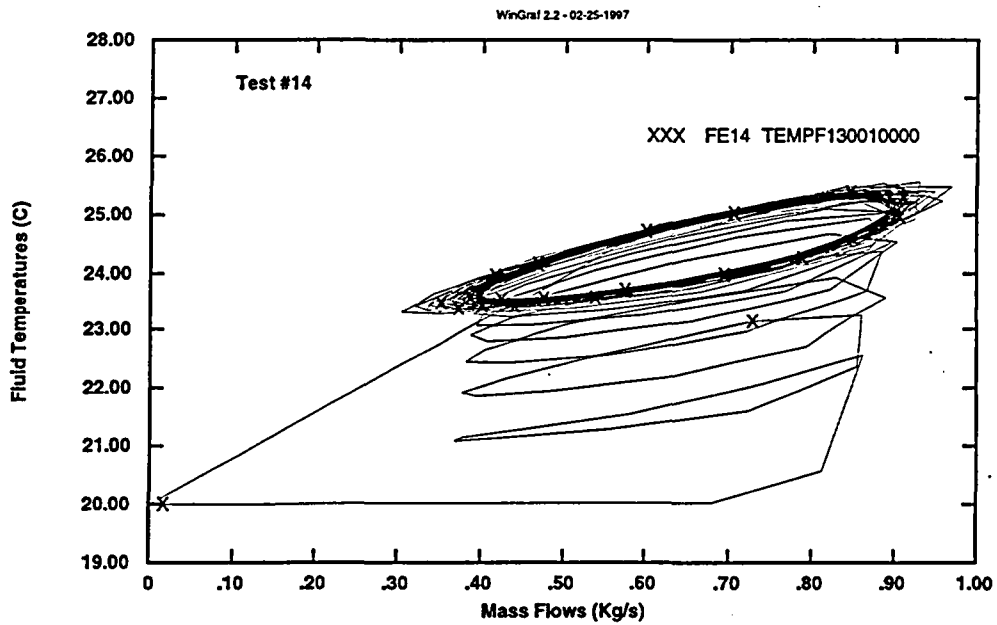


Figure C.8d TEST #14 Search for Neutral Stability.
Sink Fluid Temperature vs. Mass Flow Rate, conditions as in Figure C.8a.

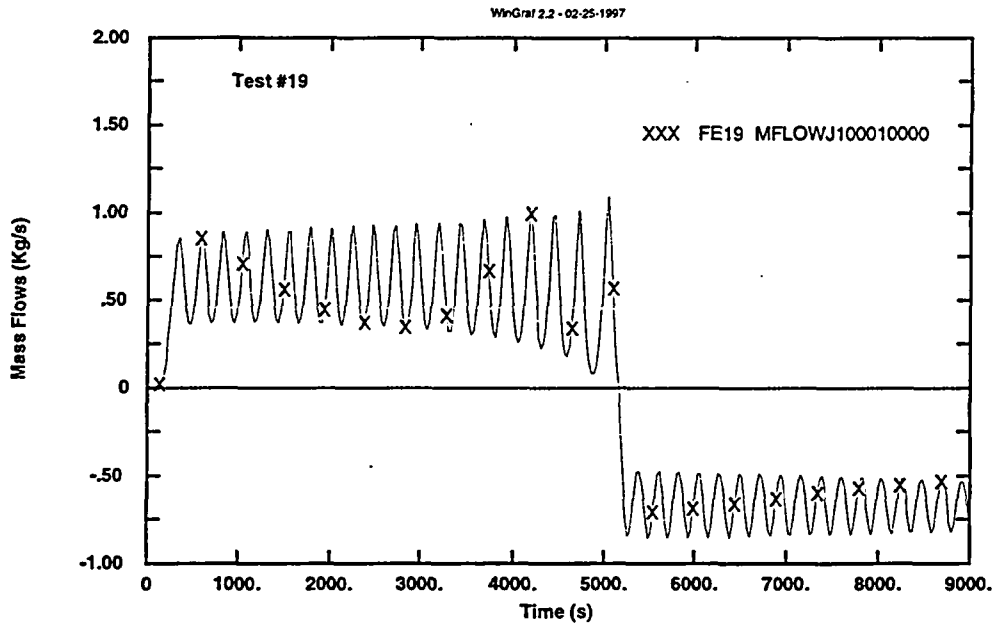


Figure C.9a TEST #19 Sensitivity of results of TDV isolation and RELAP5/MOD3.0 Mass Flow Rates in Ascending Leg, 37 nodes per leg, (Length of Components = 0.263m, Heated Length = 0.1m, Initial Mass Flow Rate=0.001Kg/s)

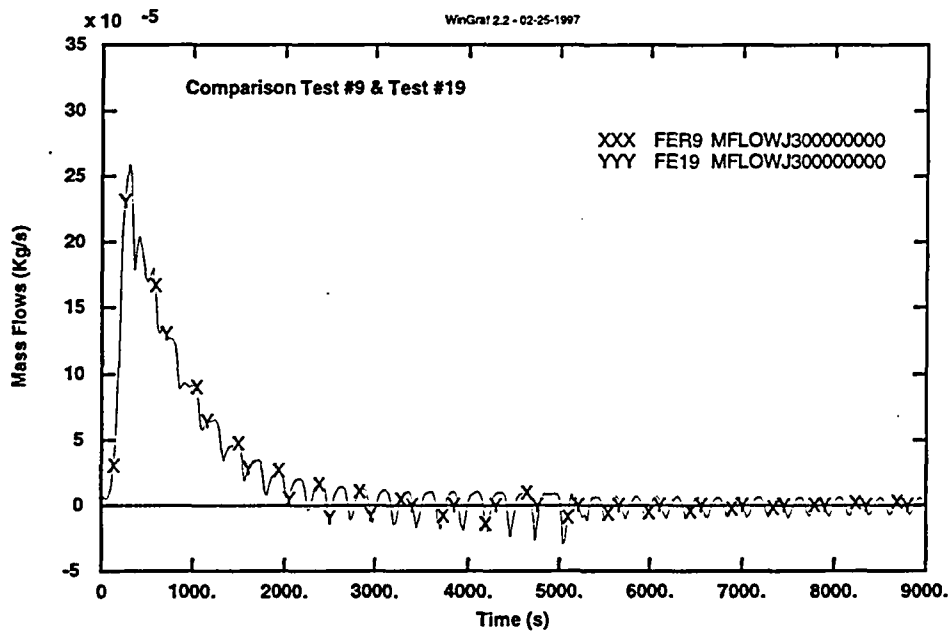


Figure C.9b TEST #19 Sensitivity of results of TDV isolation at 3000s Flow rates to/from TDV, Test #9 with valve left open up to 9000s Conditions as in Figure C9.a

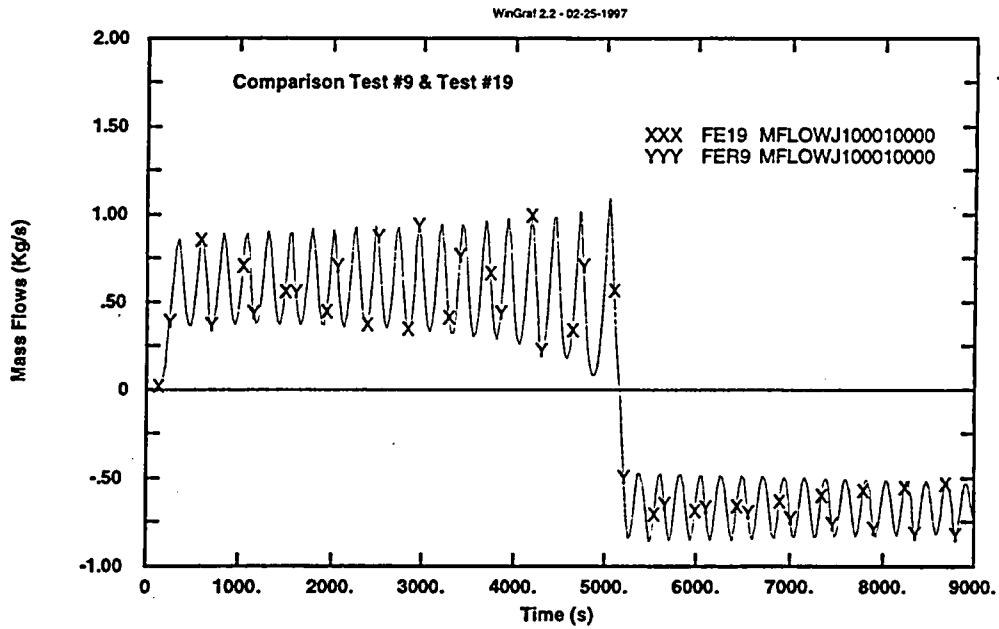


Figure C.9c TEST #19 Sensitivity of results of TDV isolation at 3000s
Flow rates in Ascending Leg, Comparison of Tests #9 and #19
Conditions as in Figure C9.a

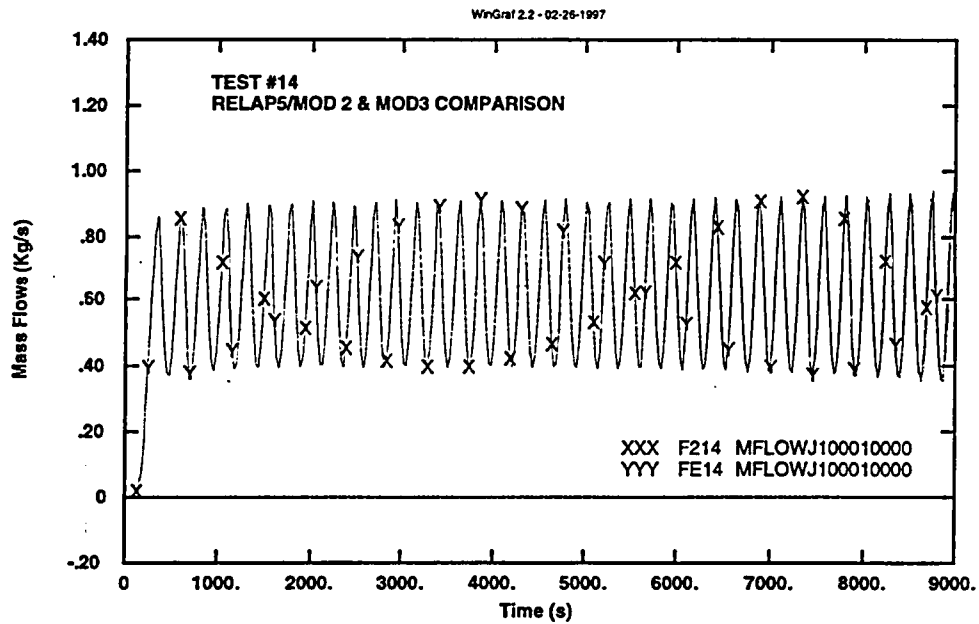


Figure C.10 TEST #14 Search for Neutral Stability, conditions as in TEST #7
Mass Flow Rates in Ascending Leg using **RELAP5/MOD3.0** and **MOD2**,
37 nodes per leg, Length of Components = 0.11m, Heated Length = 0.1m,
Initial Mass Flow Rate = 0.001Kg/s

APPENDIX D

INPUT DECK FOR WELANDER'S PROBLEM

```

*****
*
* Natural Circulation input deck for Welander's Problem
*
* Case:          alpha = 338.94 epsilon = 2.3  90 Nodes per Leg
*
100      new      transnt
*
*=====
* time steps
*
*      mint      maxt      mie      mae
201  200.      1.e-7      5.e-2      07003      500  5000  5000
202  1000.     1.e-7      5.e-2      07003      500  5000  5000
203  1.e6      1.e-7      5.e-2      07003      500  5000  5000
*
*
*      minor edit requests
*
* pressure
*
301  p          100010000      * lower plenum
302  p          130010000      * upper plenum
*
* fluid temperatures
303  tempf      100010000      * lower plenum
304  tempf      110010000      * ascending leg 1
305  tempf      110050000      * ascending leg 5
306  tempf      110100000      * ascending leg 10
310  tempf      130010000      * upper plenum
307  tempf      120100000      * descending leg 10
308  tempf      120050000      * descending leg 5
309  tempf      120010000      * descending leg 1
*
* mass flow rates
*
311  mflowj     100010000      * lower plenum to ascending leg
312  mflowj     100020000      * lower plenum to descending leg
*
*-----*
*      trips
*-----*
*
* pressure control
*
527  time  0    ge null  0      -1.          1 *
528  time  0    ge null  0      1.e06        1 *
603  527 xor 528
*
* heater temperature table
513  time  0    ge null  0      -1.e06        1 * start of heat. and cool.
*
* cooler temperature table
514  time  0    ge null  0      -1.e06        1 * start of heat. and cool.
*
* heater htc table
515  time  0    ge null  0      -1.e06        1 * constant htc
*
* cooler htc table
516  time  0    ge null  0      -1.e06        1 * constant htc
*
* end trip signal
512  time  0    ge null  0      10000.        1 * end of problem
600  512
*
*
*

```

```

*
*-----
* hydraulic components
*-----
*
* lower plenum
1000000 low.ple      branch
1000001 2           1
1000101 7.854e-03  0.1000  0.  0.  0.  0.0000 1.e-7 0.100 00000
1000200 000         1.00e5 0.10465e6 2.675e6 0.
1001101 100010000 110000000 0.  0.  0.  000000
1002101 100000000 120000000 0.  0.  0.  000000
1001201 0.99  0.  0.
1002201 -0.99 0.  0.
*
*
* ascending leg
1100000 asc.leg     pipe
1100001 90
1100101 7.854e-03  90
1100301 0.111111111111 90
1100401 0.  90
1100601 90.0 90
1100801 1.0e-7 0.0 90
1101001 00000 90
1101101 000000 89
1101201 000 1.00e5 0.106743e6 2.675e6 0.0 0. 90
1101300 1
1101301 0.99 0.000 0. 89
*
* descending leg
1200000 desc.leg    pipe
1200001 90
1200101 7.854e-03  90
1200301 0.111111111111 90
1200401 0.  90
1200601 90.0 90
1200801 1.0e-7 0.0 90
1201001 00000 90
1201101 000000 89
1201201 000 1.00e5 0.102557e6 2.675e6 0.0 0. 90
1201300 1
1201301 -0.99 0. 0. 89
*
* upper plenum
1300000 upp.ple     branch
1300001 2           1
1300101 7.854e-03  0.1000  0.  0.  0.  0.0000 1.e-7 0.100 00000
1300200 000         1.00e5 0.10465e6 2.675e6 0.
1301101 110010000 130000000 0.  0.  0.  000000
1302101 120010000 130010000 0.  0.  0.  000000
1301201 0.99  0.  0.
1302201 -0.99 0.  0.
*
* pressure control for steady state
3000000 pc.vlv      valve
3000101 130010000 400000000 7.854e-03 0.1 0.1 000100 1. 1. 1.
3000201 1 0. 0. 0.
3000300 mtrvlv
3000301 603 528 0.25 1.
*
* pressure control volume
4000000 pc.vol      tmdpvvl
4000101 0. 0.5 10. 0. 0. 0. 4.e-5 0. 00000
4000200 000
4000201 0. 1.0e5 0.084e6 2.675e6 0.
4000202 1. 1.0e5 0.084e6 2.675e6 0.
4000203 1.e6 1.0e5 0.084e6 2.675e6 0.
*

```

```

*
*-----*
*   structures
*-----*
*
* lower plenum heaters and upper plenum coolers
11001000  2   11  2  1  0.05
11001100  0    1
11001101  10  0.0501
11001201  1   10
11001301  0.  10
11001400  0
11001401 293.15 11
11001501 -900    0   1900    1   0.10    1
11001502 -901    0   1901    1   0.10    2
11001601 100010000 00000 3902    1   0.10    1
11001602 130010000 00000 3903    1   0.10    2
11001701  0    0.00    0.0    0.0    0.0    1
11001702  0    0.00    0.0    0.0    0.0    2
11001901  0. 100. 100.    0.  0.    0.  0.    1.  2
*
*-----*
* material tables
*-----*
*
*
20100100 tbl/fctn  1  1
*-----*
* heat structure conductivity
*-----*
20100101    1.0  100.
20100102 5000.0  100.
*-----*
* heat structure volumetric heat capacity
*-----*
20100151    1.0  1.e5
20100152 5000.0  1.e5
*
*-----*
* general tables
*-----*
*
*
* heater temperature
20290000 temp 513
20290001 -1.0    293.15
20290002  0.    293.15    *
20290003  0.1   303.15    *
20290004  1.e6  303.15    *
*
* cooler temperature
20290100 temp 514
20290101 -1.0    293.15
20290102  0.    293.15    *
20290103 100.1  293.15    *
20290104  1.e6  293.15    *
*
* heater htc
20290200 htc-t  515
20290201 -1.0    20000.
20290202  0.    20000.    *
20290203  0.1   20000.    *
20290204 10.0   20000.    *
20290205  1.e6  20000.    *
*

```

```
*
* cooler htc
20290300 htc-t 516
20290301 -1.0 20000.
20290302 0. 20000. *
20290303 0.1 20000. *
20290304 10.0 20000. *
20290305 1.e6 20000. *
*
*-----*
* control variables
*-----*
* none
.
```

BIBLIOGRAPHIC DATA SHEET

(See instructions on the reverse)

1. REPORT NUMBER
(Assigned by NRC, Add Vol., Supp., Rev.,
and Addendum Numbers, if any.)

NUREG/IA-0151

2. TITLE AND SUBTITLE

Verification of RELAP/MOD3 With Theoretical and Numerical Stability
Results on single-Phase, Natural Circulation in a Simple Loop

3. DATE REPORT PUBLISHED

MONTH	YEAR
February	1999

4. FIN OR GRANT NUMBER

5. AUTHOR(S)

J.C. Ferreri, ARN
W. Ambrosini, USP

6. TYPE OF REPORT

Technical

7. PERIOD COVERED *(Inclusive Dates)*

8. PERFORMING ORGANIZATION - NAME AND ADDRESS *(If NRC, provide Division, Office or Region, U.S. Nuclear Regulatory Commission, and mailing address; if contractor, provide name and mailing address.)*

Autoridad Regulatoria Nuclear
Av. del Libertador 8250
1429 Buenos Aires, Argentina

Universita degli studi Pisa, Facolta di Ingegneria
Dipartimento di Costruzioni Meccaniche e Nucleari
Via Diotisalvi 2, 56126 Pisa, Italy

9. SPONSORING ORGANIZATION - NAME AND ADDRESS *(If NRC, type "Same as above"; if contractor, provide NRC Division, Office or Region, U.S. Nuclear Regulatory Commission, and mailing address.)*

Office of Nuclear Regulatory Research
U.S. Nuclear Regulatory Commission
Washington, DC 20555-0001

10. SUPPLEMENTARY NOTES

11. ABSTRACT *(200 words or less)*

The theoretical results given by Pierre Welander are used to test the capability of the RELAP5 series of codes to predict instabilities in single-phase flow. These results are related to the natural circulation in a loop formed by two parallel adiabatic tubes with a point heat sink at the top and a point heat source at the bottom. A stability curve may be defined for laminar flow and was extended to consider turbulent flow. By a suitable selection of the ratio of the total buoyancy force in the loop to the friction resistance, the flow may show instabilities. The solution was useful to test two basic numerical properties of the RELAP5 code, namely: a) convergence to steady state flow-rate using a "lumped parameter" approximation to both the heat source and sink and, b) the effect of nodalization to numerically damp the instabilities. It was shown that, using a simple volume to lump the heat source and sink, it was not possible to reach convergence to steady state flow rate when the heated (cooled) length was diminished and the heat transfer coefficient increased to keep constant the total heat transferred to (and removed from) the fluid. An algebraic justification of these results is presented, showing that it is a limitation inherent to the numerical scheme adopted. Concerning the effect of nodalization on the damping of instabilities, it was shown that a "reasonably fine" discretization led, as expected, to the damping of the solution. However, the search for convergence of numerical and theoretical results was successful, showing the expected nearly chaotic behavior. This search lead to very refined nodalizations. The results obtained have also been verified by the use of simple, ad hoc codes. A procedure to assess the effects of nodalizations on the prediction of instabilities threshold is outlined in this report. It is based on the experience gained with the aforementioned simpler codes.

12. KEY WORDS/DESCRIPTORS *(List words or phrases that will assist researchers in locating the report.)*

RELAP5/MOD3

13. AVAILABILITY STATEMENT

unlimited

14. SECURITY CLASSIFICATION

(This Page)

unclassified

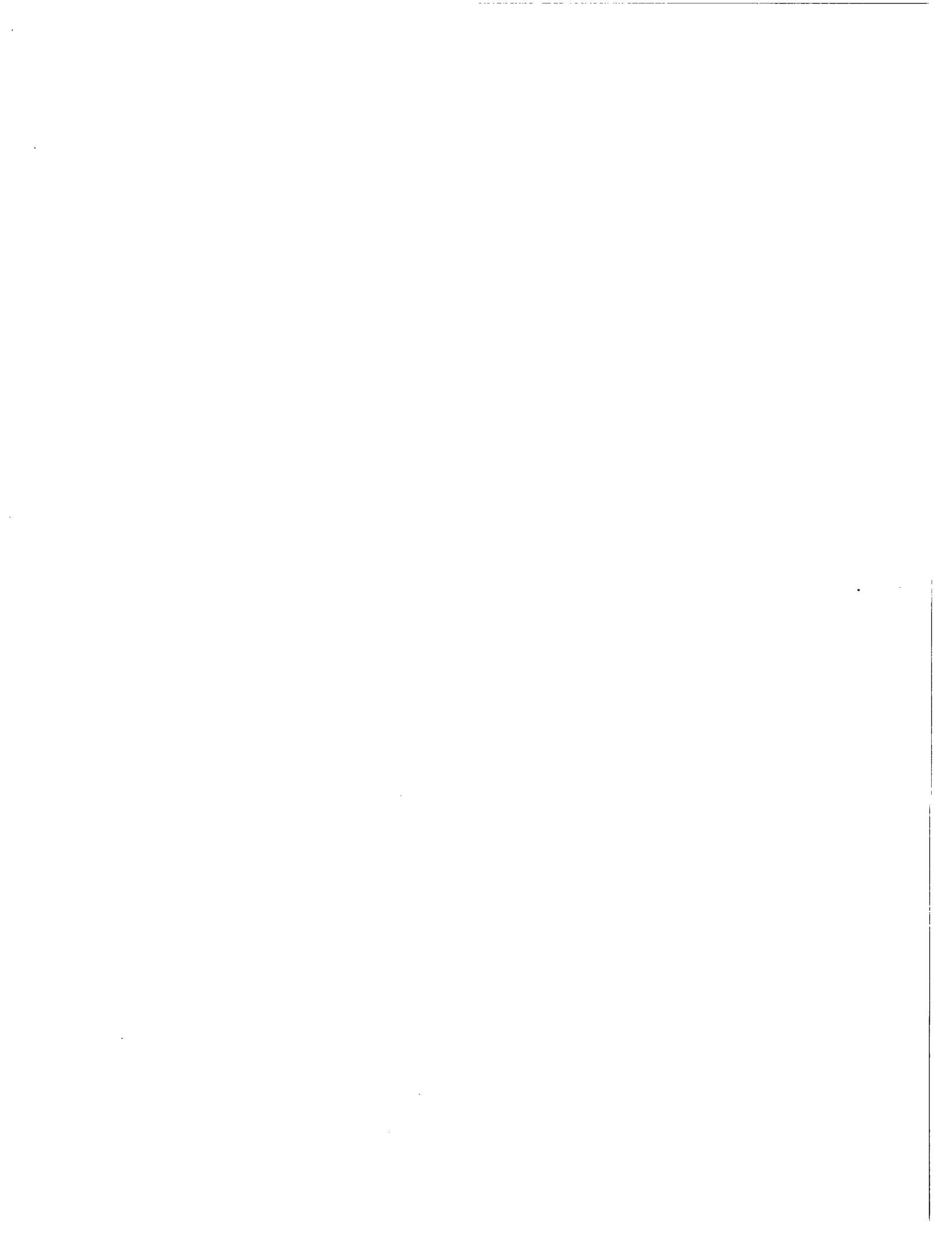
(This Report)

unclassified

15. NUMBER OF PAGES

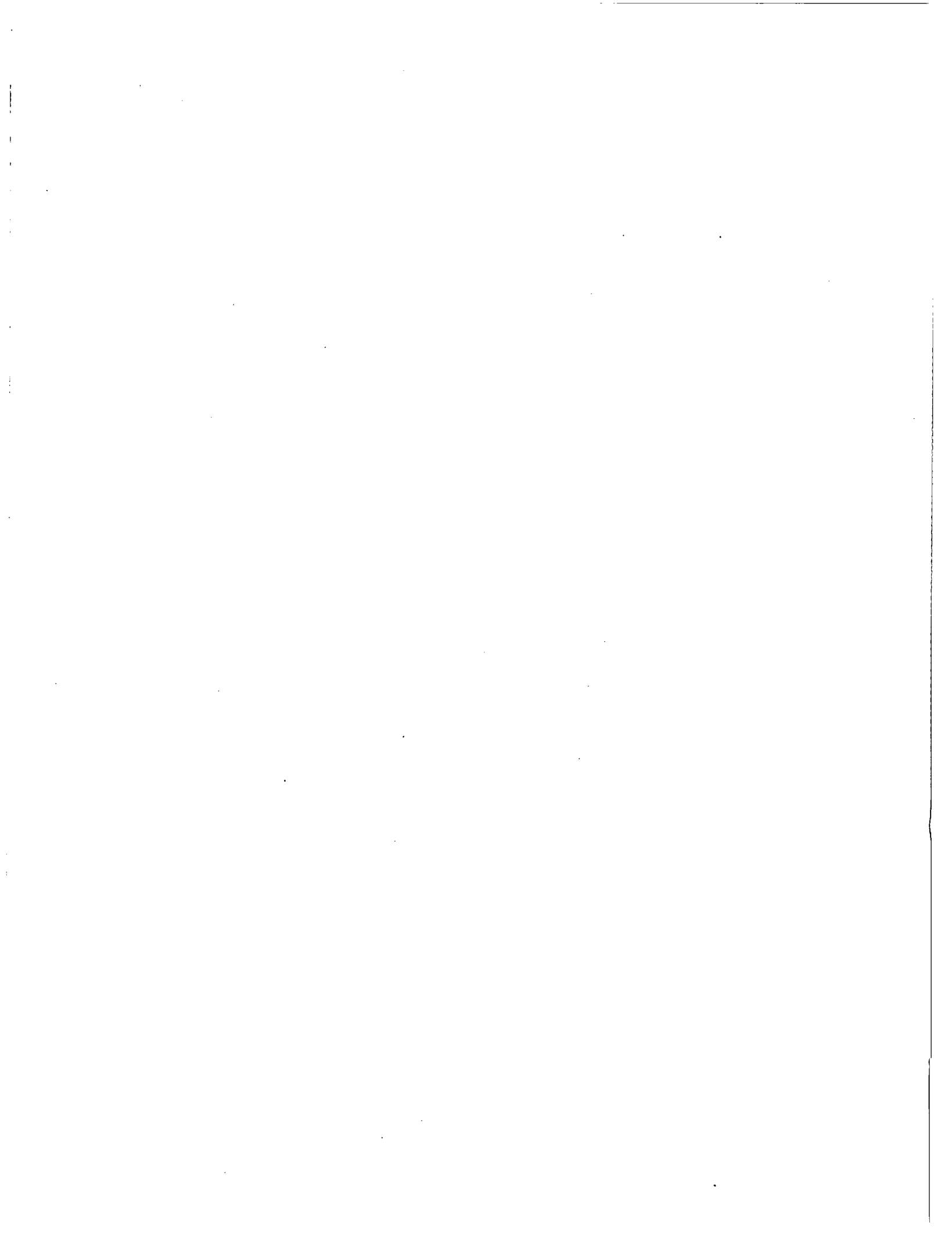
16. PRICE







Federal Recycling Program



UNITED STATES
NUCLEAR REGULATORY COMMISSION
WASHINGTON, DC 20555-0001

OFFICIAL BUSINESS
PENALTY FOR PRIVATE USE, \$300

SPECIAL STANDARD MAIL
POSTAGE AND FEES PAID
USNRC
PERMIT NO. G-67